Interaction of reactive astrocytes with type I collagen induces astrocytic scar formation through the integrin-N-cadherin pathway after spinal cord injury

原, 正光

Interaction of reactive astrocytes with collagen type I induces astrocytic scar formation through the integrin/N-cadherin pathway after spinal cord injury

Authors:

Masamitsu Hara[1,2], Kazu Kobayakawa[2], Yasuyuki Ohkawa[3], Hiromi Kumamaru[2], Kazuya Yokota[2], Takeyuki Saito[1,2], Ken Kijima[1,2], Shingo Yoshizaki[1,2], Katsumi Harimaya[2], Yasuharu Nakashima[2] and Seiji Okada[1,2]

Affiliations:

[1]Department of Advanced Medical Initiatives, Graduate School of Medical Sciences, Kyushu University, Fukuoka, Japan

[2]Department of Orthopaedic Surgery, Graduate School of Medical Sciences, Kyushu University, Fukuoka, Japan

[3]Division of Transcriptomics, Medical Institute of Bioregulation, Kyushu University, Fukuoka, Japan

Correspondence should be addressed to S.O. (seokada@ortho.med.kyushu-u.ac.jp)

Abstract

Central nervous system (CNS) injury activates naïve astrocytes into reactive astrocytes, which eventually transform into scar-forming astrocytes that can impair axonal regeneration and functional recovery. This sequential phenotypic change, known as reactive astrogliosis, has long been considered unidirectional and irreversible. However, we report here that reactive astrocytes isolated from injured spinal cords retrogradely reverted to naïve astrocytes when transplanted into a naïve spinal cord, whereas they formed astrocytic scars when transplanted into an injured spinal cord, indicating the environment-dependent reversibility of reactive astrogliosis. We also found that collagen type I was highly expressed during the scar-forming phase and induced astrocytic scar formation via the integrin/N-cadherin pathway. Pharmacological blockade of reactive astrocyte-collagen type I interaction prevented astrocytic scar formation, thereby leading to improved axonal regrowth and better functional outcomes in a mouse model of spinal cord injury. Our findings reveal environmental cues regulating astrocytic fate decisions, thereby providing a potential therapeutic target for CNS injury.

Introduction

Spinal cord injury (SCI) is a devastating trauma that causes persistent severe motor/sensory dysfunction[1,2]. After SCI, astrocytes, the most abundant resident cells in the central nervous system (CNS), play a crucial role in the SCI pathology through a phenotypic change known as reactive astrogliosis. In this process, naïve astrocytes (NAs) sequentially exhibit opposite phenotypes: first as reactive astrocytes (RAs) and then as scar-forming astrocytes (SAs). In the subacute phase of SCI (4-14 days post-injury (dpi) in the mouse), RAs migrate to the lesion epicenter and seclude inflammatory cells, leading to tissue repair and functional improvement after SCI[2]. However, RAs gradually transform into SAs that form astrocytic scars, the main impediment for CNS axonal regeneration, resulting in a limited functional recovery in the chronic phase of SCI[3,4] (more than 14 dpi in the mouse). Astrocytic scars have been shown to be irreversible and permanently inhibit axonal regrowth in both rodents and humans with SCI[4-6], although there is a different opinion that attenuating astrocytic scar formation failed to promote axonal regeneration after SCI[7,8]. As such, clarifying the mechanism of astrocytic scar formation and regulating this scar formation may be a potential therapeutic strategy for SCI.

Astrocytic scars have been studied for more than half a century[9,10], and their formation has been suggested to be regulated by complex and combinatorial inter- and intra-cellular signaling mechanisms[3,5,11]. However, despite the large number of studies examining these astrocytic changes[5,11,12], the mechanism underlying astrocytic scar formation remains unclear. One factor limiting basic research in this area is the lack of clear definitions of NAs, RAs, and SAs. A conventional method for distinguishing between these cells is a histological analysis, but this method is neither objective nor quantitative.

In this study, we established a clear distinction between NAs, RAs, and SAs based on marker gene expression and investigated the regulatory mechanism underlying astrocytic scar

formation after SCI.

Results

In situ isolation of astrocytes after SCI enables the discovery of RA- and SA-specific marker genes

We employed the contusion SCI model in female C57BL/6J mice (8-10 weeks old). This approach is reported to resemble human SCI more closely than transection models, because most human SCI are due to blunt trauma[13]. After SCI, NAs exhibited drastic changes around the lesion area (**Supplementary Fig. 1a**). They underwent a typical change of hypertrophy, process extension and increased GFAP expression within several dpi, characteristic of RAs (**Supplementary Fig. 1b**)[2]. Thereafter, at 14 dpi, the RAs overlapped and transformed into SAs, resulting in astrocytic scar formation (**Supplementary Fig. 1b**)[3,12]. Although this sequential astrocytic transformation is roughly referred to as “reactive astrogliosis”, identifying the point at which the astrocytes are situated in this process is difficult: RAs and SAs both highly express their hallmark protein (GFAP, Nestin, β-catenin, N-cadherin and Sox9), but clearly distinguishing between each form of astrocytes (NAs, RAs, and SAs) based solely on their hallmark expression is difficult with a histological analysis (**Supplementary Fig. 2a**,**b**, **Supplementary Fig. 3a**,**b**)[12,14-16].

Therefore, we selectively isolated each astrocyte type by laser microdissection (LMD) combined with immunohistochemistry: NAs, morphologically identical to resident astrocytes in the naïve spinal cord; RAs, with the morphological characteristics described above (observed in the injured spinal cord at 7 dpi); and SAs, scar-forming GFAP-positive cells observed in the injured spinal cord at 14 dpi in a mouse model of contusion SCI (**Fig. 1a-g**). Excellent RNA qualities as well as no contamination of other cell type were confirmed with a bioanalyzer and a PCR analysis in the collected samples of astrocytes (**Fig. 1h, i**). We investigated the expression levels of RA- and SA-characteristic genes that were reported previously, and

defined the specific genes both significantly and selectively upregulated in LMD-isolated NAs, RAs and SAs as their respective marker genes.

Regarding RAs, we confirmed elevated gene expressions of *Gfap*, *Nes*, *Vim*, and *Ctnnb1* (encoding β-catenin) compared with NAs. However, increased expressions of *Gfap* and *Vim* were also observed in SAs, indicating that only *Nes* and *Ctnnb1* were suitable as RA marker genes (**Fig. 1j**). In addition, we found the β-catenin-related genes suitable as RA markers from a functional aspect. In SCI, RA migration is crucial for both functional and tissue repair[2], and recent reports have suggested a possible molecular link between β-catenin and cell movement via MMPs[17,18]. After β-catenin nuclear translocation, the β-catenin-LEF/TCF complex binds the enhancer of urokinase-type plasminogen activator receptor (uPAR) gene, resulting in the activation of MMPs and cell migration. We demonstrated selectively elevated expression of *Plaur* (encoding uPAR), *Mmp2*, and *Mmp13* in RAs compared with NAs and SAs (**Fig. 1j**). Furthermore, the expression of *Axin2*, a negative feedback regulator of β-catenin, was significantly higher in RAs than in NAs or SAs (**Fig. 1j**). These results show that *Plaur*, *Mmp2*, *Mmp13*, and *Axin2* as well as *Nes* and *Ctnnb1* are suitable as RA marker genes, providing further insight into the mechanism of RA migration through β-catenin/MMPs signaling.

Regarding SAs, we confirmed significantly elevated expression of *Cdh2* (encoding N-cadherin) and *Sox9* compared with NAs and RAs (**Fig. 1k**). We also detected significantly higher expression of chondroitin sulfate proteoglycan (CSPG)-related genes, such as *Xylt1*, *Chst11*, *Csgalnact1*, *Acan*, and *Pcan*, in SAs than in NAs and RAs (**Fig. 1k**). These results were biologically plausible, because CSPGs are the most abundant extracellular inhibitor of axonal regeneration, and their expression has been selectively observed in the astrocytic scar area after SCI[3,12,16,19]. In addition, the strong repulsive axon guidance gene *slit2*[3,20] was also found to be suitable as a SA marker gene (**Fig. 1k**). These marker gene profiles combined with

the morphological definitions are useful for identifying the astrocyte phenotypes present, as reactive astrogliosis is a graded continuum of changes in gene expression and forms.

Dependence of reactive astrogliosis on the surrounding environment

The phenotypic changes in mammalian cells are roughly driven in a cell-autonomous or a non-cell-autonomous manner[21,22]; however, the mechanism of reactive astrogliosis remains unclear. To clarify the mechanism, we prepared GFP-positive NAs from primary astrocyte cultures of *CAG-EGFP* mice and transplanted them into the spinal cord of either naïve mice or immediately after spinal contusion in SCI mice (**Fig. 2a**, **Supplementary Fig. 4a-c**). At 7 and 14 days after transplantation (dat), we examined morphological transformations of the grafted NAs in response to the environment (**Fig. 2b**). The morphology of transplanted NAs, such as the cell diameter and ratio of cells with overlapping of neighboring astrocytic processes, was unchanged in the naïve spinal cord, whereas they had transformed along with the host astrocytic changes and were integrated into reactive astrogliosis when transplanted into the injured spinal cord (**Fig. 2c-j**).

In addition to these morphological changes, we examined the sequential changes in the gene expression by a cell-selective analysis of grafted NAs using LMD (**Fig. 3a**,**b**). Consistent with the morphological transition, gene expression of the grafted NAs remained unchanged when transplanted into the naïve spinal cord, whereas the expression of the RA marker genes at 7 dat and SA marker genes at 14 dat were significantly increased compared to those at other time points when transplanted into the injured spinal cord (**Fig. 3c**,**d**). These findings indicate that astrocytes change their phenotypes in an environment-dependent manner (**Supplementary Fig. 5a**).

Reversibility of reactive astrogliosis

After confirming the environment-dependent properties of reactive astrogliosis after SCI, we examined the reversibility of the sequential astrocytic changes and whether or not RAs could retrogradely revert to NAs after transplantation into naïve spinal cord. To selectively isolate RAs, we developed *Nes-Cre*; *CAG-CAT*$^{loxP/loxP}$*-EGFP* (*Nes-EGFP*) mice, which show selective EGFP expression in RAs upon Cre-mediated recombination[2]. We confirmed that these mice showed no GFP-positive cells in the naïve spinal cord, but had high Cre-mediated EGFP expression in RAs around the lesion area at 7 dpi in SCI mice (**Supplementary Fig. 6a-d**, **Fig. 4a**,**b**). After dissociating the injured spinal cords of *Nes-EGFP* mice at 7 dpi, we selectively isolated the GFP-positive RAs by fluorescence-activated cell sorting (FACS) and confirmed significantly increased expressions of the RA marker genes in the isolated RAs (**Supplementary Fig. 7a**,**b**). We then transplanted these GFP-positive RAs into either naïve or injured spinal cord models and performed immunohistological and cell-selective gene expression analyses with LMD at 7 dat (**Fig. 4c**,**d**). The grafted RAs formed astrocytic scars when transplanted into the injured spinal cord but histologically reverted to NAs when transplanted into the naïve spinal cord at 7 dat. (**Fig. 4e-h**). Consistent with this morphological conversion, a selective gene expression analysis of the grafted cells demonstrated that the SA marker gene expressions were upregulated when transplanted into the injured spinal cord, while the original expression patterns of SA marker genes were significantly suppressed when transplanted into the naïve spinal cord (**Fig. 4i**). Moreover, the whole transcriptome analysis of isolated RAs, transplanted RAs in the naïve spinal cord at 7 dat, and host astrocytes in the naïve spinal cord, revealed that the global gene expression profile of transplanted and host astrocytes was comparable, while it was markedly different from isolated RAs (**Fig. 4j**, **Supplementary Fig. 8a**), suggesting that the *in situ* phenotype reprogramming of astrocytes depended on the

environment. These results clearly indicate that the process of reactive astrogliosis is reversible under certain conditions (**Supplementary Fig. 9a**).

Upregulation of collagen type I genes in the lesion area after SCI

RAs are beneficial, while SAs are harmful for the repair process after SCI; as such, preventing the transformation of RAs to SAs through environmental regulation may be a new therapeutic strategy for SCI. Given that grafted RAs reverted to NAs in the naïve spinal cord but transformed into SAs in the injured spinal cord, the fate of RAs seems to be determined by environmental differences between the naïve and injured spinal cord.

We therefore performed a time-course genome-wide expression analysis in naïve and injured spinal cord models after SCI, as described in our previous studies[23,24]. The scatter plots showed both the upregulation and downregulation of all genes between the naïve and injured groups (**Fig. 5a**). The expressions of nearly 5% of the genes were considerably increased in the injured spinal cord at 14 dpi compared to those in the naïve spinal cord (>5-fold change; **Fig. 5a**). We originally expected that the genes involved in intracellular signaling or cytokines guiding cell transformation would be enriched in the scar-forming phase of SCI. However, interestingly, a GO term analysis showed that the genes associated with the extracellular matrix (ECM) were highly enriched at 14 dpi, indicating the involvement of the ECM in scar formation after SCI (**Fig. 5b**). Among the ECM genes, the collagen type I (Col I) genes (*Col1a1* and *Col1a2*) were the most highly expressed in the injured spinal cord at 14 dpi (**Fig. 5c**). In addition, the mRNA expressions of Col I genes were significantly greater in the injured spinal cord than in the naïve spinal cord (**Fig. 5d**). Furthermore, in immunohistochemistry, the Col I expression was abundantly observed at the lesion area at 14 dpi in the injured spinal cord but not in the naïve spinal cord (**Fig. 5e**). Interestingly, astrocytic scars were formed by SAs colocalizing with Col

I; however, the RAs retained their phenotypes in the Col I-absent area at 14 dpi (**Fig. 5e-g**). These findings suggest that Col I is directly involved in the transformation of RAs into SAs as well as astrocytic scar formation after SCI.

Induction of N-cadherin-mediated adhesion by collagen type I in astrocytes

To clarify the influence of Col I on RA fate determination, we cultured RAs *in vitro* on Col I-coated dishes (Col I-coated group) or non-coated dishes (non-coated group) and performed an immunocytological analysis. While the RAs of the non-coated group showed process retraction and decreased GFAP expression, the RAs of the Col I-coated group adhered closely to the adjacent cells and showed increased GFAP expression, exhibiting a phenotype similar to that of SAs (**Fig. 5h**). In addition, we found significantly increased expression of N-cadherin, characteristic of SA, in only the Col I-coated group (**Fig. 5h**,**i**). Given that astrocytes form N-cadherin-mediated adhesion[25,26] and that N-cadherin upregulation had been observed at astrocytic scars (**Supplementary Fig. 3a**)[15], these results suggest that Col I enhances N-cadherin-mediated contacts in RAs and induces their transformation into SAs.

Induction of astrocytic transformation by the collagen type I-integrin axis

For ECM proteins, including Col I, their counterpart receptors are necessary in order to interact with cells[27]. Among ECM receptors, α1β1, α2β1, α10β1, and α11β1 integrin are reported to be a major class of collagen-binding integrins that play an important role in cell-Col I interaction[27]. Since these collagen-binding integrins are expressed on astrocytes[28,29], we speculated that they directly mediated the RA-Col I interaction and induced the transformation into SAs. We therefore analyzed the morphological and gene expression changes in RAs of the Col I-coated group treated with or without anti-collagen-binding integrin antibody (anti-β1 Ab) (**Fig. 6a**).

Notably, the RAs treated with control Ab showed cell adhesion and the increased expression of N-cadherin and GFAP, while those treated with anti-β1 Ab remained scattered with no change in the expression of N-cadherin or GFAP (**Fig. 6b**,**c**). Similarly, N-cadherin neutralizing antibody (N-cadherin nAb) inhibited the transformation of RAs into SAs under the same conditions (**Supplementary Fig. 10a**). These results suggest that Col I induces the transformation of RAs into SAs via the integrin/N-cadherin pathway, indicating a potential therapeutic target.

Prevention of astrocytic scar formation and amelioration of functional recovery after SCI via the blockade of RA-collagen type I interaction

Therapeutically, whether or not preventing the transformation of RAs into SAs can indeed attenuate astrocytic scar formation after SCI is particularly important, because axons cannot regenerate beyond astrocytic scars, thereby limiting the functional recovery[3,4,6,12]. We investigated the effects of inhibition of integrin-mediated RA-Col I interaction on *in vivo* astrocytic scar formation and functional recovery after SCI (**Fig. 6a**).

Anti-β1 Ab was administered from 9 to 13 dpi after SCI in order to selectively attenuate the transformation of RAs to SAs (**Fig. 6d**). At 14 dpi in the anti-β1 Ab injection group, we observed significantly lower expression of both N-cadherin and GFAP at the lesion area, resulting in reduced cell adhesion and astrocytic scar formation compared to the control group (**Fig. 6e**,**f**). We also confirmed that the injection of N-cadherin nAb attenuated astrocytic scar formation similarly to the administration of anti-β1 Ab (**Supplementary Fig. 10b-d**). Regarding the axonal regrowth, immunostaining using an antibody against GAP43, a marker for regenerating axons, showed that the number of GAP43-positive axons was significantly increased at both the lesion epicenter and the caudal area of the lesion in mice treated with anti-

β1 Ab compared with those treated with control Ab (**Fig. 6g**,**h**). The numbers of serotonin (5-HT)-positive and tyrosine hydroxylase (TH)-positive fibers in mice treated with anti-β1 Ab were also larger in comparison to mice treated with control Ab, and most of these fibers in mice with anti-β1 Ab expressed GAP43 (**Supplementary Fig. 11a-d**). These results indicate that the number of regenerative fibers passing through the lesion epicenter was significantly increased by the attenuation of astrocytic scar formation. To investigate whether or not these regenerating axons contribute to the behavioral improvements, we performed an open-field locomotor test and a footprint analysis, and demonstrated that the motor functional recovery with anti-β1 Ab injection was significantly greater than that achieved with control Ab injection (**Fig. 6i-l**). These results indicate that the inhibition of integrin-mediated RA-Col I interaction prevents astrocytic scar formation via N-cadherin downregulation and promotes the axonal regeneration and functional recovery after SCI.

Discussion

Astrocytic scars, the final form of reactive astrogliosis, are widely regarded as a principal cause for axonal regrowth failure and a poor functional outcome[3,12]. Reactive astrogliosis has long been considered unidirectional and irreversible in the SCI pathology[2,4,5]. However, our findings conversely showed the environment-dependent reversibility of reactive astrogliosis, highlighting the therapeutic potential of regulating this astrocytic change through environmental intervention. In particular, a time-course RNA-seq analysis identified Col I as a prominent factor for the scar-forming phase of SCI, and Col I was crucial for astrocytic scar formation via the integrin/N-cadherin pathway. Furthermore, the blockade of RA-Col I interaction attenuated astrocytic scar formation and promoted functional improvement after SCI, providing a novel therapeutic target for the treatment of SCI.

Using LMD, we demonstrated for the first time the *in vivo* transcriptional profiles of NAs, RAs, and SAs and defined their marker genes. FACS or translating ribosomal affinity purification (TRAP) have thus far been mainly used for cell-specific analyses[23,30]; however, LMD had an advantage over these methods in our study. While FACS and TRAP require the separation of solid organ tissues into single cells[31], LMD makes it possible to capture cells while maintaining and observing cell-specific structures[32]. Therefore, LMD combined with immunohistochemistry was indispensable for selectively isolating each form of astrocyte based on the recognition of their antigens and morphologies, because the astrocytes exhibited phenotypic heterogeneity around the SCI lesion (**Supplementary Fig. 1a**, **Fig. 5f-h**).

Although the completed astrocytic scars strongly inhibit the regenerative response after CNS injury, RAs, transitional form of reactive astrogliosis, play beneficial roles in the subacute phase of SCI, in processes such as local immune regulation, neuroprotection, and tissue repair[33-36]. In addition to the definition of astrocytic marker genes, a cell-selective analysis with

LMD demonstrated that the signaling pathways related to these beneficial functions were activated in RAs (**Fig. 1j**, **Supplementary Fig. 12a**). For example, the β-catenin/MMPs pathway was reported to be involved in astrocytic migratory activity as well as tissue repair after SCI. TGF-β signaling contributes to both the neuronal survival and axonal regeneration[37,38]. PDGF reduces the inflammatory response by enhancing the phagocytic activity of microglia/macrophages after SCI[39]. We found that these pathways were significantly and selectively activated in RAs, providing deeper insight into the beneficial influence of RAs on tissue repair and functional recovery after SCI.

As shown in **Figs. 5** and **6**, we demonstrated that Col I was involved in the N-cadherin-mediated cell-cell adhesion in astrocytes through integrin signaling and astrocytic scar formation. To date, pericytes and fibroblasts have been reported to be the cell types that produce Col I after SCI[12,40,41], and we actually confirmed that these cells were clearly merged with Col I in the lesion epicenter (**Supplementary Fig. 13a,b**). Regarding a possible molecular link between the Col I-integrin axis and increased N-cadherin-dependent contact in astrocytes, c-Jun-N-terminal kinase (JNK) may play a role. In previous studies of epithelial and cancer cells, the Col I-integrin axis was reported to activate the downstream JNK pathway, which influenced the N-cadherin-dependent intercellular adhesion[42,43]. Similarly, in astrocytes, Col I-integrin axis stimulation was recently reported to induce JNK activation[44], and upregulation of both JNK and N-cadherin has been observed in astrocytes after CNS injury (**Supplementary Fig. 3a**)[15,45,46]. Given that JNK inhibitor attenuates astrocytic scar formation in the injured spinal cord[47], the integrin/JNK/N-cadherin pathway is crucial for astrocytic scar formation after SCI. In this study, we also confirmed both attenuated astrocytic scar formation via Col I-integrin axis inhibition by anti-β1 Ab as well as an improved functional outcome (**Fig. 6d-l**), providing a novel potential therapeutic target for SCI.

N-cadherin regulated reactive astrogliosis by increasing the astrocytic cell-cell adhesion. N-cadherin belongs to the classic cadherins that are calcium-dependent intercellular adhesion molecules[25,26] and has many functions in the CNS, such as differentiation, migration, and cell polarization[25,26,48]. In addition to cell adhesion, N-cadherin in astrocytes has also been reported to be involved in the migratory activity and cellular morphology. For example, both a lack of and the overexpression of N-cadherin result in the impairment of astrocytic migration[48,49]. Kanemura et al. also reported that astrocyte-specific knockout of N-cadherin results in insufficient morphological changes in both RAs and SAs after CNS injury[48]. These results indicate that the N-cadherin expression in astrocytes is finely tuned through the process of reactive astrogliosis. Indeed, we confirmed the time-phase-dependent expression of N-cadherin concomitant with cellular hypertrophy and process extension in RAs and SAs (**Fig. 1k**, **Fig. 5h**, **Fig. 6b**,**e**, **Supplementary Fig. 3a**). Although both anti-β1 Ab and N-cadherin nAb prevented the transformation of RAs into SAs and attenuated astrocytic scar formation in this study, there is a possibility that N-cadherin nAb impairs the beneficial function of RA more severely than anti-β1 Ab, since N-cadherin has significant influence on the cellular morphology and migration of RA as described above. We therefore used anti-β1 Ab. In the present study, anti-β1 was administered during only the scar-forming phase to attenuate scar formation without influencing the morphological changes or migratory activity of RAs. Our results have important implications for the optimization of therapeutic intervention from the time-phase-dependent view of reactive astrogliosis.

Regarding the role of astrocytic scars after SCI, Anderson et al. recently reported that the attenuation of astrocytic scar formation failed to result in spontaneous axonal regrowth after SCI[7,8], suggesting that astrocytic scar formation aids axonal regeneration. However, the impairment of “the whole process of reactive astrogliosis” has already been reported to cause

the deterioration of axonal regrowth and functional recovery after SCI in several previous studies[3,50,51], and there has been no study demonstrating that astrocytic "scars" directly promote axonal regeneration after SCI. In contrast, Silver and many other investigators demonstrated that astrocytic "scars" directly impede axonal regeneration[3-6,12,51], and our results supported this finding. In this study, we therefore prevented only the transformation of RAs into SAs without affecting RAs, leading to axonal elongation and functional improvement after SCI. These findings suggest the significance of the time-phase-dependent regulation of reactive astrogliosis for the SCI treatment.

In conclusion, we demonstrated the reversibility of reactive astrogliosis by a selective gene expression analysis with LMD and transplantation experiments. We also clarified a mechanism of astrocytic scar formation through RA-Col I interaction, supporting a novel therapeutic strategy for attenuating astrocytic scar formation and improving the functional outcomes after SCI.

Acknowledgements

We thank T. Tachibana for the gift of anti-Nestin antibody. This study was supported by a Grant-in-Aid for Young Scientist (A) (25713053) (S.O.); Challenging Exploratory Research from the Ministry of Education, Science, Sports (16K15668) (S.O.); a Grant-in-Aid for Young Scientist (B) (16K20059) (K.Kobayakawa); Scientific Research on Innovative Areas (Comprehensive Brain Science Network and Foundation of Synapse Neurocircuit Pathology) (K.Kobayakawa); and research foundations from the general insurance association of Japan (M.H.),.

Author contributions

M.H. designed and performed most of the experiments with technical help from H.K., T.S., and S.Y. Y.O. performed the RNA-Seq analysis. K.Y. and K. Kijima analyzed the data of LMD. K. Kobayakawa, K.H. and Y.N. designed the studies and supervised the overall project. S.O. designed the studies, supervised the overall project, and performed the final manuscript preparation.

Competing financial interests

The authors declare no competing financial interests.

References

1. McDonald, J. W. & Sadowsky, C. Spinal-cord injury. *Lancet* **359,** 417–425 (2002).
2. Okada, S. *et al.* Conditional ablation of Stat3 or Socs3 discloses a dual role for reactive astrocytes after spinal cord injury. *Nat. Med.* **12,** 829–834 (2006).
3. Silver, J. & Miller, J. H. Regeneration beyond the glial scar. *Nat. Rev. Neurosci.* **5,** 146–156 (2004).
4. Karimi-Abdolrezaee, S. & Billakanti, R. Reactive astrogliosis after spinal cord injury-beneficial and detrimental effects. *Mol. Neurobiol.* **46,** 251–264 (2012).
5. Ridet, J. L., Malhotra, S. K., Privat, A. & Gage, F. H. Reactive astrocytes: cellular and molecular cues to biological function. *Trends Neurosci.* **20,** 570–577 (1997).
6. Buss, A. *et al.* Gradual loss of myelin and formation of an astrocytic scar during Wallerian degeneration in the human spinal cord. *Brain* **127,** 34–44 (2004).
7. Anderson, M. A. *et al.* Astrocyte scar formation aids central nervous system axon regeneration. *Nature* **532,** 195–200 (2016).
8. Liddelow, S. A. & Barres, B. A. Regeneration: Not everything is scary about a glial scar. *Nature* **532,** 182–183 (2016).
9. Windle, W. F., Clemente, C. D. & Chambers, W. W. Inhibition of formation of a glial barrier as a means of permitting a peripheral nerve to grow into the brain. *J. Comp. Neurol.* **96,** 359–369 (1952).
10. Freeman, L. W. Return of Spinal Cord Function in Mammals After Transecting Lesions. *Ann. N. Y. Acad. Sci.* **58,** 564–569 (1954).
11. Sofroniew, M. V. Molecular dissection of reactive astrogliosis and glial scar formation. *Trends Neurosci.* **32,** 638–647 (2009).
12. Cregg, J. M. *et al.* Functional regeneration beyond the glial scar. *Exp. Neurol.* **253,**

197–207 (2014).

13. Courtine, G. *et al.* Can experiments in nonhuman primates expedite the translation of treatments for spinal cord injury in humans? *Nat. Med.* **13,** 561–566 (2007).

14. Renault-Mihara, F. *et al.* Beneficial compaction of spinal cord lesion by migrating astrocytes through glycogen synthase kinase-3 inhibition. *EMBO Mol. Med.* **3,** 682–696 (2011).

15. Vázquez-Chona, F. & Geisert, E. E., J. N-cadherin at the glial scar in the rat. *Brain Res.* **838,** 45–50 (1999).

16. McKillop, W. M., Dragan, M., Schedl, A. & Brown, A. Conditional Sox9 ablation reduces chondroitin sulfate proteoglycan levels and improves motor function following spinal cord injury. *Glia* **61,** 164–177 (2013).

17. Mann, B. *et al.* Target genes of beta-catenin-T cell-factor/lymphoid-enhancer-factor signaling in human colorectal carcinomas. *Proc. Natl. Acad. Sci. U. S. A.* **96,** 1603–1608 (1999).

18. Blasi, F. & Carmeliet, P. uPAR: a versatile signalling orchestrator. *Nat. Rev. Mol. Cell Biol.* **3,** 932–943 (2002).

19. Takeuchi, K. *et al.* Chondroitin sulphate N-acetylgalactosaminyl-transferase-1 inhibits recovery from neural injury. *Nat. Commun.* **4,** 2740 (2013).

20. Hagino, S. *et al.* Slit and glypican-1 mRNAs are coexpressed in the reactive astrocytes of the injured adult brain. *Glia* **42,** 130–138 (2003).

21. Ilieva, H., Polymenidou, M. & Cleveland, D. W. Non-cell autonomous toxicity in neurodegenerative disorders: ALS and beyond. *J. Cell Biol.* **187,** 761–772 (2009).

22. von Karstedt, S. *et al.* Cancer cell-autonomous TRAIL-R signaling promotes KRAS-Driven cancer progression, invasion, and metastasis. *Cancer Cell* **27,** 561–573 (2015).

23. Kumamaru, H. *et al.* Direct isolation and RNA-seq reveal environment-dependent properties of engrafted neural stem/progenitor cells. *Nat. Commun.* **3,** 1140 (2012).

24. Kumamaru, H. *et al.* Therapeutic activities of engrafted neural stem/precursor cells are not dormant in the chronically injured spinal cord. *Stem Cells* **31,** 1535–1547 (2013).

25. Takeichi, M. The cadherin superfamily in neuronal connections and interactions. *Nat. Rev. Neurosci.* **8,** 11–20 (2007).

26. Tran, M. D., Wanner, I. B. & Neary, J. T. Purinergic receptor signaling regulates N-cadherin expression in primary astrocyte cultures. *J. Neurochem.* **105,** 272–286 (2008).

27. Hynes, R. O. Integrins: Bidirectional, Allosteric Signaling Machines. *Cell* **110,** 673–687 (2002).

28. Previtali, S. C., Archelos, J. J. & Hartung, H. P. Modulation of the Expression of Integrins on Cells during Experimental Autoimmune Encephalomyelitis. A Central Role for TNF-alpha. *Am. J. Pathol.* **151,** 1425–1435 (1997).

29. Yonezawa, T. *et al.* Type IV collagen induces expression of thrombospondin-1 that is mediated by integrin alpha1beta1 in astrocytes. *Glia* **58,** 755–767 (2010).

30. Doyle, J. P. *et al.* Application of a Translational Profiling Approach for the Comparative Analysis of CNS Cell Types. *Cell* **135,** 749–762 (2008).

31. Garg, A. *et al.* Non-enzymatic dissociation of human mesenchymal stromal cells improves chemokine-dependent migration and maintains immunosuppressive function. *Cytotherapy* **16,** 545–559 (2014).

32. Yokota, K. *et al.* Engrafted Neural Stem/Progenitor Cells Promote Functional Recovery through Synapse Reorganization with Spared Host Neurons after Spinal Cord Injury. *Stem Cell Reports* **5,** 264–277 (2015).

33. Faulkner, J. R. *et al.* Reactive astrocytes protect tissue and preserve function after spinal cord injury. *J. Neurosci.* **24,** 2143–2155 (2004).

34. Rolls, A. *et al.* Two faces of chondroitin sulfate proteoglycan in spinal cord repair: a role in microglia/macrophage activation. *PLoS Med.* **5,** e171 (2008).

35. Rolls, A., Shechter, R. & Schwartz, M. The bright side of the glial scar in CNS repair. *Nat. Rev. Neurosci.* **10,** 235–241 (2009).

36. Shechter, R., Raposo, C., London, A., Sagi, I. & Schwartz, M. The glial scar-monocyte interplay: A pivotal resolution phase in spinal cord repair. *PLoS One* **6,** e27969 (2011).

37. Brionne, T. C., Tesseur, I., Masliah, E. & Wyss-Coray, T. Loss of TGF-β 1 Leads to Increased Neuronal Cell Death and Microgliosis in Mouse Brain. *Neuron* **40,** 1133–1145 (2003).

38. Abe, K., Chu, P. J., Ishihara, A. & Saito, H. Transforming growth factor-β 1 promotes re-elongation of injured axons of cultured rat hippocampal neurons. *Brain Res.* **723,** 206–209 (1996).

39. Lutton, C. *et al.* Combined VEGF and PDGF Treatment Reduces Secondary Degeneration after Spinal Cord Injury. *J. Neurotrauma* **29,** 957–970 (2012).

40. DePaul, M. A., Lin, C. Y., Silver, J. & Lee, Y. S. Peripheral Nerve Transplantation Combined with Acidic Fibroblast Growth Factor and Chondroitinase Induces Regeneration and Improves Urinary Function in Complete Spinal Cord Transected Adult Mice. *PLoS One* **10,** e0139335 (2015).

41. Goritz, C. *et al.* A Pericyte Origin of Spinal Cord Scar Tissue. *Science.* **333,**

238–242 (2011).

42. Shintani, Y., Wheelock, M. J. & Johnson, K. R. Phosphoinositide-3 Kinase-Rac1-c-Jun NH_2-terminal Kinase Signaling Mediates Collagen I-induced Cell Scattering and Up-Regulation of N-Cadherin Expression in Mouse Mammary Epithelial Cells. *Mol. Biol. Cell* **17,** 2963–2975 (2006).

43. Shintani, Y., Hollingsworth, M. A., Wheelock, M. J. & Johnson, K. R. Collagen I Promotes Metastasis in Pancreatic Cancer by Activating c-Jun NH_2-Terminal Kinase 1 and Up-regulating N-Cadherin Expression. *Cancer Res.* **66,** 11745–11753 (2006).

44. Le Dréau, G. *et al.* NOV/CCN3 Upregulates CCL2 and CXCL1 Expression in Astrocytes Through β1 and β5 Integrins. *Glia* **58,** 1510–1521 (2010).

45. Cao, J., Wang, J. S., Ren, X. H. & Zang, W. D. Spinal sample showing p-JNK and P38 associated with the pain signaling transduction of glial cell in neuropathic pain. *Spinal Cord* **53,** 92–97 (2015).

46. Gao, K. *et al.* Traumatic Scratch Injury in Astrocytes Triggers Calcium Influx to Activate the JNK/c-Jun/AP-1 Pathway and Switch on GFAP Expression. *Glia* **61,** 2063–2077 (2013).

47. Repici, M. *et al.* Specific inhibition of the JNK pathway promotes locomotor recovery and neuroprotection after mouse spinal cord injury. *Neurobiol. Dis.* **46,** 710–721 (2012).

48. Kanemaru, K. *et al.* Calcium-dependent N-cadherin up-regulation mediates reactive astrogliosis and neuroprotection after brain injury. *Proc. Natl. Acad. Sci.* **110,** 11612–11617 (2013).

49. Péglion, F. & Etienne-Manneville, S. N-cadherin expression level as a critical indicator of invasion in non-epithelial tumors. *Cell Adhes. Migr.* **6,** 327–332 (2012).

50. Bush, T. G. *et al.* Leukocyte infiltration, neuronal degeneration, and neurite outgrowth after ablation of scar-forming, reactive astrocytes in adult transgenic mice. *Neuron* **23,** 297–308 (1999).

51. Silver, J. The glial scar is more than just astrocytes. *Exp. Neurol.* **286,** 147–149 (2016).

Figure legends

Figure 1. Selective *in situ* isolation and gene expression analysis of astrocytes from the naïve and injured spinal cords. (a, **c** and **e**) Example images depicting GFAP (green) staining of the naïve (**a**) and injured spinal cords at 7 (**c**) and 14 (**e**) dpi. The asterisk indicates the lesion epicenter in SCI mice (**c** and **e**). Scale bars, 500 μm. (**b**, **d** and **f**) Example high magnification images depicting immunohistochemical analysis of GFAP-positive astrocytes (green) stained with Hoechst (blue) in the naïve (**b**) and injured spinal cords at 7 (**d**) and 14 (**f**) dpi. The arrowheads and dashed-outlines indicate the astrocytes before (left) and after (right) LMD. The images are magnifications of the boxed areas in (**a**), (**c**) and (**e**), respectively. Scale bars, 50μm. (**g**) A schematic representation of the selective isolation of GFAP-positive astrocytes using LMD. (**h**) Bioanalyzer gel image (left) and electropherogram with the associated RNA integrity number (RIN) values (right) of RNA from LMD-isolated astrocytes. (**i**) Example PCR analysis of selected transcripts in whole spinal cord (top) and LMD-isolated astrocytes (bottom). (**j**) Quantification of mRNA expression levels of RA-related genes in NAs, RAs, and SAs (n = 4 mice per group). (**k**) Quantification of mRNA expression levels of SA-related genes in NAs, RAs, and SAs (n = 4 mice per group). $^{\star}P < 0.05$, analysis of variance (ANOVA) with the Tukey-Kramer post hoc test (**j** and **k**); n.s., not significant. Data represent mean ± SEM.

Figure 2. Environment-dependent morphological changes of NAs transplanted into naïve or injured spinal cords. (**a** and **b**) The NA transplantation protocol. NAs from primary astrocyte cultures of *CAG-EGFP* mice were transplanted into the naïve and injured spinal cord immediately after SCI. An immunohistochemical (IHC) analysis of the grafted NAs was performed at 0, 7, and 14 dat. (**c**, **e** and **g**) Example images depicting IHC analysis of GFP-positive NAs (green) transplanted into the naïve spinal cord at 7 dat (**c**) and the injured spinal

cord at 7 (**e**) and 14 (**g**) dat, stained with GFAP (red). The asterisk indicates the lesion epicenter in SCI mice (**e** and **g**). Scale bars, 500 μm. (**d**, **f** and **h**) Example high magnification images depicting IHC analysis of GFP-positive grafted NAs (green) stained with GFAP (red) and Hoechst (blue) in the naïve spinal cords at 7 dat (**d**) and the injured spinal cords at 7 (**f**) and 14 (**h**) dat. The images are magnifications of the boxed areas in (**c**), (**e**) and (**g**), respectively. Scale bars, 50μm. (**i**) A morphometric analysis of the cell diameter in host or GFP-positive transplanted astrocytes in naïve or injured spinal cords (n = 8 mice per group). (**j**) The percentage of host or GFP-positive transplanted astrocytes with overlapping of neighboring astrocytic processes in naïve or injured spinal cords (n = 8 mice per group). Wilcoxon's rank sum test (**i** and **j**); n.s., not significant. Data represent mean ± SEM.

Figure 3. Environment-dependent transcriptional profiles of NAs transplanted into naïve or injured spinal cords. (**a** and **b**) The NA transplantation and selective isolation protocol. NAs from primary astrocyte cultures of *CAG-EGFP* mice were transplanted into naïve or injured spinal cords immediately after SCI. GFP-positive grafted NAs were selectively isolated by LMD for a gene expression analysis at 0, 7, and 14 dat. The arrowheads and dashed-outlines indicate the astrocytes before (left) and after (right) LMD. Scale bar, 50 μm (**a**). (**c** and **d**) Time-course quantification of mRNA expression levels of RA (**c**) and SA marker genes (**d**) in NAs transplanted into naïve or injured spinal cords (n = 4 mice per group). Gene expression levels were normalized to that of the NAs transplanted into the naïve spinal cord at 0 dat. $^{\star}P < 0.05$, ANOVA with the Tukey-Kramer post hoc test; n.s., not significant. Data represent mean ± SEM.

Figure 4. Reversibility of reactive astrogliosis depends on the surrounding spinal cord environment. (a) Example images depicting GFP (green) staining of the sagittal section of

Nes-EGFP mice at 7 dpi after SCI. The asterisk indicates the lesion epicenter in SCI mice. Scale bar, 500 μm. (**b**) Example high magnification images depicting immunostaining of GFP (green), GFAP (red), and Nestin (blue) triple-positive RAs in the perilesional area of *Nes-EGFP* mice at 7 dpi. The asterisk indicates the lesion epicenter in SCI mice. Scale bar, 50 μm. (**c** and **d**) The protocol showing selective isolation and transplantation of RAs. (**e** and **f**) Example high magnification images depicting immunostaining of the GFP-positive RAs (green) transplanted into naïve or injured spinal cords at 7 dat, stained with GFAP (red) and Hoechst (blue). The asterisk indicates the lesion epicenter in SCI mice (**e**). Scale bars, 50 μm. (**g**) A morphometric analysis of the cell diameter in host or GFP-positive transplanted astrocytes in naïve or injured spinal cords (n = 8 mice per group). (**h**) The ratio of host or GFP-positive transplanted astrocytes with overlapping of neighboring astrocytic processes in naïve or injured spinal cords (n = 8 mice per group). (**i**) Time-course quantification of mRNA expression levels of SA marker genes in RAs transplanted into naïve or injured spinal cords (n = 4 mice per group). Gene expression levels were normalized to that of NAs in the naïve spinal cord of *Nes-EGFP* mice. (**j**) The hierarchical clustering of the whole transcriptome analysis data from RAs, transplanted astrocytes and host astrocytes (n = 3 mice per group). The values indicate Pearson's correlation coefficients. $^{\star}P < 0.05$, ANOVA with the Tukey-Kramer post hoc test (**g**, **h** and **i**); n.s., not significant. Data represent mean ± SEM.

Figure 5. RNA-seq analysis reveals the role of Col I in the induction of N-cadherin-dependent adhesion in RAs. (**a**) Scatter plots between the naïve and injured spinal cord (n = 1 mice per group). These represent many overexpressed (>5-fold change) genes (red). (**b**) A GO term analysis of the overexpressed (> 5-fold change) genes in the RNA-seq analysis of the injured spinal cord (14 dpi) compared to those of the naïve spinal cord (n = 1 mice per group).

The lists show the top seven obtained GO terms ranked by *p*-value (Fisher's exact test with the Benjamini-Hochberg correction). (**c**) The FPKM values of the top 20 extracellular matrix genes at 14 dpi (n = 1 mice per group). (**d**) Quantification of mRNA expression levels of the Col I genes (*Col1a1* and *Col1a2*) of spinal cords before injury and at 14 dpi (n = 4 mice per group). (**e**, **f**, and **g**) Example images depicting immunostaining of the naïve and injured spinal cord at 14 dpi, stained with GFAP (green), Col I (red), and Hoechst (blue). The asterisk indicates the lesion epicenter in SCI mice (**e**). Scale bars, 100 μm (**e**), 50 μm (**f** and **g**). (**h**) Example images depicting immunocytochemical analysis of the RAs on the non-coated or Col I-coated dishes, stained with GFAP (green), N-cadherin (red), and Hoechst (blue). Scale bar, 50 μm. (**i**) Quantification of *Cdh2* mRNA expression levels in the RAs on the non-coated or Col I-coated dishes (n = 4 wells per group). $^{\star}P < 0.05$, Wilcoxon's rank sum test (**d** and **i**). Data represent mean ± SEM.

Figure 6. Inhibition of integrin-mediated RA-Col I interaction prevents astrocytic scar formation and promotes functional recovery after SCI. (**a**) A schematic representation of the SA transformation induced by the Col I/integrin/N-cadherin pathway. Anti-β1 Ab blocks the Col I-integrin axis in RAs. (**b**) Example images depicting immunocytochemical analysis of RAs on Col I-coated dishes after anti-β1 Ab or control Ab administration, stained with GFAP (green), N-cadherin (red), and Hoechst (blue). Scale bar, 50 μm. (**c**) Quantification of *Cdh2* mRNA expression levels in RAs after anti-β1 Ab or control Ab administration (n = 4 wells per group). Gene expression levels were normalized to that of the RAs on non-coated dishes without any Ab administration. (**d**) The schedule of *in vivo* anti-β1 Ab injection to wild-type mice after SCI. (**e**) Example images depicting IHC analysis of the injured cords receiving anti-β1 Ab or control Ab injection, stained with GFAP (green), N-cadherin (red), and Hoechst (blue).

The asterisk indicates the lesion epicenter in SCI mice. Scale bar, 50 μm. (**f**) The ratio of GFAP-positive astrocytes with overlapping of neighboring astrocytic processes in the lesion area of SCI mice after anti-β1 Ab or control Ab administration (n = 8 mice per group). (**g**) Example images depicting GAP43 (white) and Col I (red) staining of the injured cords receiving anti-β1 Ab or control Ab injection at 42 dpi. Scale bars below the images, 200 μm, insets 40μm. (**h**) Quantification of GAP43-positive area per 4.0×10^5 μm^2 (n = 8 mice per group). (**i**) Time course of the BMS score after SCI (n = 12 mice per group). (**j**) Example images depicting footprint analysis at 42 dpi. (**k**) Quantification of the footprint analysis findings in each mouse (n = 8 mice per group). (**l**) Scores for the grip walk test at 42 dpi (n = 8 mice per group). $^{\star}P < 0.05$, $^{\star\star}P < 0.005$, ANOVA with the Tukey-Kramer post hoc test (**c**), Wilcoxon's rank sum test (**f**, **h**, **k** and **l**), and two-way repeated measures ANOVA with the Tukey-Kramer post hoc test (**i**). Data represent mean ± SEM.

Online Methods

Animals

All animal studies were approved by the Committee of Ethics on Animal Experimentation of the Faculty of Medicine, Kyushu University. The experiments were conducted in accordance with the National Institutes of Health guidelines for the care and use of animals. Female C57BL/6J mice (8–10 weeks old) were used in this study. *CAG-EGFP* mice, *Nes-Cre* mice, and *CAG-CAT$^{loxP/loxP}$-EGFP* mice were as described previously[2,52]. To generate *Nes-Cre*; *CAG-CAT$^{loxP/loxP}$-EGFP* (*Nes-EGFP*) mice, we crossed *Nes-Cre* mice and *CAG-CAT$^{loxP/loxP}$-EGFP* mice.

Primary astrocyte cultures

Purified primary astrocyte cultures were prepared from *CAG-EGFP* mice or C57BL/6J mice, as described previously[2,53]. In brief, after the removal of the meninges, postnatal day 2 mouse brain tissues were minced and incubated in a rocking water bath at 37 °C for 30 min in Dulbecco's modified Eagle's medium (DMEM; Invitrogen, Carlsbad, California) in the presence of 0.25% trypsin (Sigma-Aldrich) and 300 g ml^{-1} DNase I (Sigma-Aldrich). The dissociated cells were triturated with 0.25% fetal bovine serum (FBS) and centrifuged at 300 × *g* for 5 min. Following dilution with astrocyte-specific medium (DMEM containing 10% FBS, 0.2 mML-glutamine, and 1% penicillin-streptomycin), the cells were plated on non-coated culture dishes. After 7-10 days in a humidified CO_2 incubator at 37 °C, the astrocytes were used for experiments. For the activation to RAs, the astrocytes were stimulated with 50 ng ml^{-1} IL-6 (R&D Systems Inc.) and 200 ng ml^{-1} soluble IL-6 receptor (R&D Systems Inc.). For the preparation of Col I-coated dishes, the dishes were incubated at 37 °C for 2 h with mouse collagen type I (50 μg ml^{-1}; AbD Serotec), as described previously[54].

Spinal cord injury

The animals were anesthetized via an intraperitoneal injection of pentobarbital (75 mg kg^{-1}) and subjected to a contusion injury (70 kilodyne) at the 10th thoracic level using an Infinite Horizons Impactor (Precision Systems Instrumentation)[32]. During the period of recovery from anesthesia, the mice were placed in a temperature-controlled chamber until thermoregulation was reestablished.

Flow cytometry and cell sorting

The spinal cord samples (4 mm in length, centered around the lesion) were dissociated in collagenase type I (Invitrogen), followed by an analysis using a cell sorter, SH800 (Sony), as described previously[23,55]. GFP-positive RAs isolated from the injured spinal cord of *Nes-EGFP* mice were used for transplantation.

Cell transplantation

Using a stereotaxic injector (KDS 310; Muromachi-kikai), a 25-μl Hamilton syringe (Hamilton) with a glass tip was inserted into the injured spinal cord (1 mm rostral to the lesion epicenter) or the naïve spinal cord. A total volume of 2 μl of cell suspension (2.0×10^4 viable cells per microliter) was injected at a rate of 0.5 μl min^{-1}.

Behavioral analyses

The motor function was evaluated with a locomotor open-field rating scale on the Basso Mouse Scale (BMS)[32]. A footprint analysis was also performed, as described previously[32]. The forelimbs and hindlimbs of the mice were dipped in red and green dyes, respectively. For the

grip walk test, a grid walk was reconstructed for mice using two parallel pieces of wood. After 3 days of training, each mouse was evaluated using 50 cm of the grid with three patterns: easy (50 steps, 1 cm apart), medium (every third step removed), and hard (every other step removed)[24]. The sum of the number of grips for all three patterns was calculated in the analysis. All tests were performed in a double-blinded fashion.

Histopathological examination

After the animals were reanesthetized and transcardially fixed with 4% paraformaldehyde, the spinal cord was removed, dehydrated, and embedded in an OCT compound. The frozen sections were cut in the sagittal plane at 16 μm or the axial plane at 20 μm. The sections were subsequently stained with primary antibodies in the blocking solution at 4 °C overnight and then incubated with Alexa Fluor secondary antibodies 1 (1:200; Invitrogen) and Hoechst 33258. The following primary antibodies were used: GFAP (1:200, rabbit; Dako, Z0334), GFAP (1:200, rat; Life Technologies, 130300), Nestin (1:200, rat; a gift from Dr. Taro Tachibana, Osaka City University, Osaka, Japan), β-catenin (1:200, mouse; Millipore, 05-665), N-cadherin (1:200, mouse; BD Transduction Laboratories, 610921), Sox9 (1:200, rabbit; Abcam, ab26414), COL1A1 (1:200, mouse; Sigma-Aldrich, SAB1402151), GAP-43 (1:200, rabbit; Novus Biologicals, NB300-143), serotonin (5-HT; 1:200, goat; ImmunoStar, 20079), tyrosine hydroxylase (TH; 1:200, mouse; Millipore, MAB318), platelet-derived growth factor receptor β (PDGFRβ; pericyte marker, 1:200, rabbit; Abcam, ab32570), ER-TR7 (fibroblast marker, 1:200, rat, Santa Cruz Biotechnology, sc-73355). The GAP43-positive, 5-HT-positive or TH-positive area per 4.0×10^5 μm^2 at 42 dpi was measured using the BZ-II analyzer software program (Keyence). We randomly selected 20 cells in each sample and measured the astrocyte cell diameter or ratio of cells with overlapping of neighboring astrocytic processes using the

Image J software program (U.S. National Institutes of Health). All images were captured using a BZ-9000 digital microscope system (Keyence) or epifluorescence microscope equipped with a digital camera (BX51; 12 Olympus).

Laser-capture microdissection

Fresh spinal cords were immediately frozen in dry ice/hexane and stored in a deep freezer at -80 °C. The tissues were cut at 16 μm using a cryostat at -20 °C and mounted on PEN membrane slides. The sections were then fixed in ice-cold acetone for 2 min and stained with the antibody against GFAP (1:50, rabbit; Dako) for 5 min. GFP-positive RAs and GFAP-positive astrocytes were dissected with an LMD 6500 system (Leica Microsystems) and transferred by gravity into separate microcentrifuge tube caps placed directly beneath the section. The tube caps were then filled with 75 μl of RLT buffer (Qiagen). For each sample, 1000 cells were dissected from 1 series of sagittal sections and subjected to RNA extraction.

Reverse transcription (RT)-PCR

Total RNA was isolated from the astrocytes obtained from the spinal cord tissue using the RNeasy Micro Kit (Qiagen) or from the injured spinal cord (4 mm in length) using the RNeasy Mini Kit (Qiagen). For the complementary DNA (cDNA) synthesis, a reverse transcription reaction was performed using a PrimeScript first-strand cDNA Synthesis Kit (Takara Bio). Quantitative RT-PCR was performed using primers specific to the genes of interest (Table S1) and SYBR Premix Dimmer-Eraser (Takara Bio). The data were normalized to the expression of glyceraldehyde-3-phosphate dehydrogenase. RT-PCR was conducted using a Thermocycler (Biometra), and the products were detected by electrophoresis and ethidium bromide staining.

RNA sequencing

The sample preparation and data analyses were performed as described previously[56]. In brief, the mRNA-seq library was prepared using the NEBNext Ultra Directional Library Prep Kit for Illumina (NEB) and sequenced on an Illumina HiSeq-1500 system. The sequence reads were aligned to the mouse reference genome (mm9, build 37), and the gene expression (fragments per kilobase of exon per million mapped sequence reads; FPKM) was calculated using the TopHat (version 2.0.11) and Cufflinks (version 2.1.1) software programs[57]. The selected genes of interest were converted into lists of GO terms on GO database annotations with DAVID[58]. The calculated $-\log_{10}$ (*P*-values) are displayed on the x-axis of the graph.

The sequencing and data analysis (CEL-Seq2)

We performed CEL-Seq2 for the whole transcriptome analysis of RAs (isolated by FACS at 7 dpi), transplanted and host astrocytes (both isolated by LMD at 7 dat), in accordance with a previously described protocol[59]. We sequenced the libraries using an Illumina MiSeq system. The reads were mapped to the mouse reference genome (mm10) using the Bowtie 2 software program (version 2.2.6)[60]. Pearson's correlation coefficients were calculated using the common logarithm of the read counts for genes with non-zero counts in at least one sample. Differentially expressed genes (DEGs) were extracted using the DESeq2 library (version 1.10.1) for R (with adjusted p-values of < 0.1)[61].

Anti-β1 Ab injection

SCI mice received an injection of 1 μg function-blocking monoclonal antibody against β1-integrin (anti-β1 Ab; BD Pharmingen, 555003) at the epicenter using a stereotaxic injector (KDS 310; Muromachi-kikai) every 2 days from 9 to 13 dpi. Control mice were given an

equivalent amount of isotype control (control Ab; BD Pharmingen, 553958). For *in vitro* blocking of collagen-integrin signaling, anti-β1 Ab or control Ab was added at 1 μg ml^{-1}, and an immunocytological analysis and mRNA extraction were performed at 12 h after administration.

The administration of N-cadherin nAb

We injected 10 μg of neutralizing monoclonal antibody against N-cadherin (N-cadherin nAb; Sigma-Aldrich, C3865) at the lesion epicenter in SCI mice using a stereotaxic injector (KDS 310; Muromachi-kikai) every 2 days from 9 to 13 dpi. Control mice received an equivalent amount of isotype control IgG (control IgG; BioXCell, BE0083). For the *in vitro* N-cadherin blockade experiments, N-cadherin nAb or control IgG was added at 10 μg ml^{-1}, and an immunocytological analysis was performed at 12 h after administration.

Statistical analysis

Wilcoxon's rank-sum test was used to compare the medians of the data of qPCR, the cell diameter, the ratio of overlapping-positive cells, the GAP43-positive, 5-HT-positive or TH-positive area, and the functional outcome scores. For multiple comparisons in qPCR, an analysis of variance (ANOVA) with the Tukey-Kramer post hoc test was applied. For the analysis of the differences in the BMS scores between the groups over time, a two-way repeated measures ANOVA with the Tukey-Kramer post hoc test was performed. In all statistical analyses, the level of significance was set at 0.05. The values for groups are presented as the average ± SEM. All of the statistical analyses were carried out using the JMP software program (version 11; SAS Institute).

Data availability

RNA-seq (whole spinal cords) and CEL-Seq2 (isolated astrocytes) data are deposited with accession codes DRA004535 (DDBJ) and DRA005561 (DDBJ), respectively.

Methods-only References

52. Okabe, M., Ikawa, M., Kominami, K., Nakanishi, T. & Nishimune, Y. `Green mice' as a source of ubiquitous green cells. *FEBS Lett.* **407,** 313–319 (1997).

53. Sanai, N. *et al.* Unique astrocyte ribbon in adult human brain contains neural stem cells but lacks chain migration. *Nature* **427,** 740–744 (2004).

54. Takahashi, S. *et al.* C-type lectin-like domain and fibronectin-like type II domain of phospholipase A_2 receptor 1 modulate binding and migratory responses to collagen. *FEBS Lett.* **589,** 829–835 (2015).

55. Hayashi, M. *et al.* Chd5 Regulates MuERV-L/MERVL Expression in Mouse Embryonic Stem Cells Via H3K27me3 Modification and Histone H3.1/H3.2. *J. Cell. Biochem.* **117,** 780–792 (2016).

56. Harada, A. *et al.* Incorporation of histone H3.1 suppresses the lineage potential of skeletal muscle. *Nucleic Acids Res.* **43,** 775–786 (2015).

57. Trapnell, C. *et al.* Differential gene and transcript expression analysis of RNA-seq experiments with TopHat and Cufflinks. *Nat. Protoc.* **7,** 562–578 (2012).

58. Dennis, G., Jr. *et al.* DAVID: Database for Annotation, Visualization, and Integrated Discovery. *Genome Biol.* **4,** P3 (2003).

59. Hashimshony, T. *et al.* CEL-Seq2: sensitive highly-multiplexed single-cell RNA-Seq. *Genome Biol.* **17,** 77 (2016).

60. Langmead, B. & Salzberg, S. Fast gapped-read alignment with Bowtie 2. *Nat Methods.* **9**, 357-359 (2012).

61. Love, M. I., Huber, W. & Anders, S. Moderated estimation of fold change and dispersion for RNA-seq data with DESeq2. *Genome Biol.* **15**, 550 (2014).

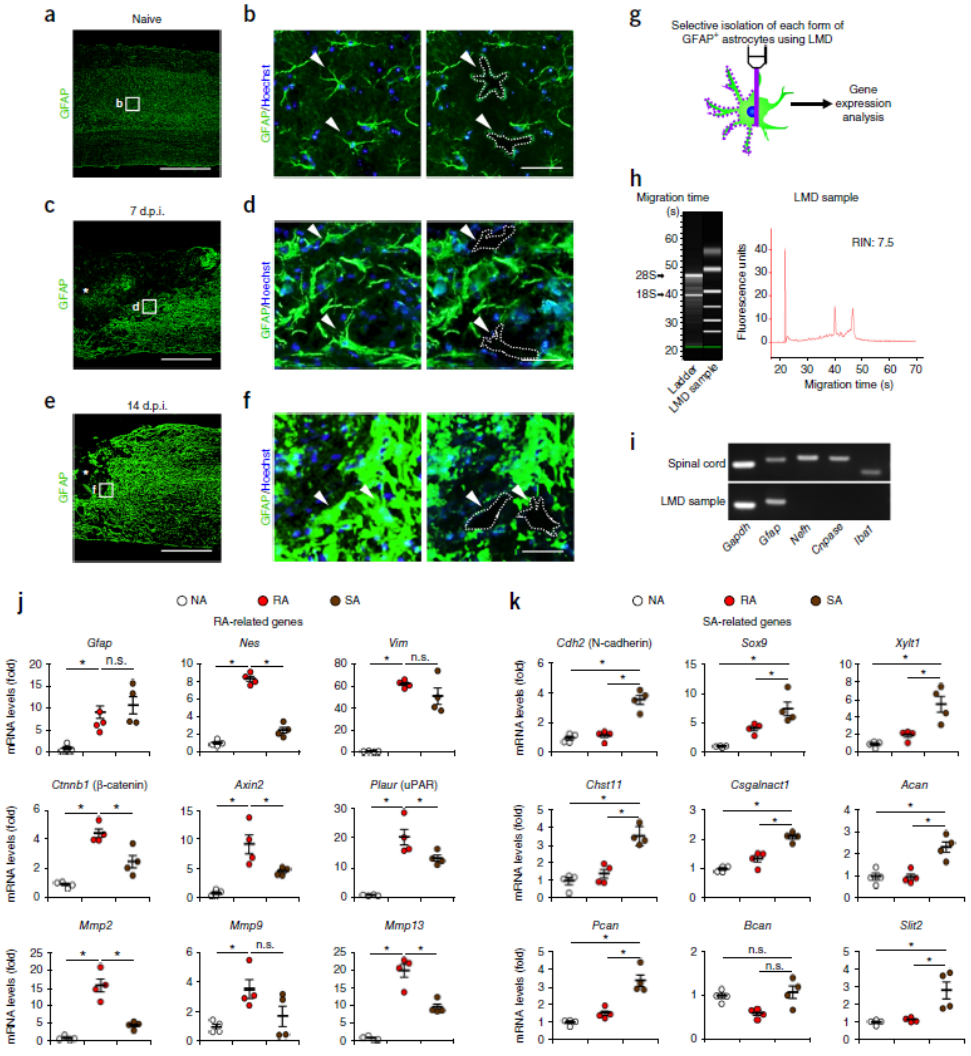
a
Naive
GFAP
b
GFAP/Hoechst
c
7 d.p.i.
GFAP
d
GFAP/Hoechst
e
14 d.p.i.
GFAP
f
GFAP/Hoechst
g
Selective isolation of each form of GFAP+ astrocytes using LMD
Gene expression analysis
h
Migration time (s)
LMD sample
RIN: 7.5
28S
18S
Ladder
LMD sample
Fluorescence units
Migration time (s)
i
Spinal cord
LMD sample
Gapdh
Gfap
Nefh
Caspase
Iba1
j
NA
RA
SA
RA-related genes
Gfap
Nes
Vim
Ctnnb1 (β-catenin)
Axin2
Plaur (uPAR)
Mmp2
Mmp9
Mmp13
n.s.
mRNA levels (fold)
k
NA
RA
SA
SA-related genes
Cdh2 (N-cadherin)
Sox9
Xylt1
Chst11
Csgalnact1
Acan
Pcan
Bcan
Slit2
n.s.
mRNA levels (fold)

Figure 1.

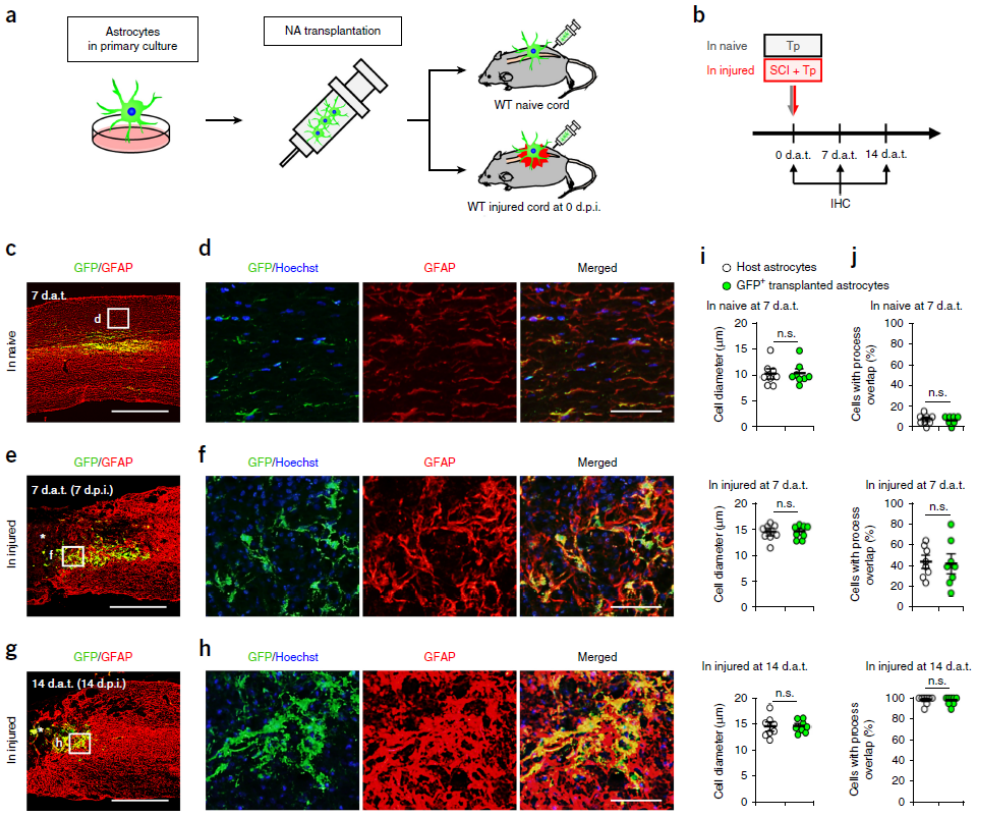
a
Astrocytes in primary culture
NA transplantation
WT naive cord
WT injured cord at 0 d.p.i.
b
In naive
In injured
Tp
SCI + Tp
0 d.a.t.
7 d.a.t.
14 d.a.t.
IHC
c
d
GFP/GFAP
GFP/Hoechst
GFAP
Merged
In naive
7 d.a.t.
e
f
7 d.a.t. (7 d.p.i.)
In injured
g
h
14 d.a.t. (14 d.p.i.)
i
Host astrocytes
GFP+ transplanted astrocytes
In naive at 7 d.a.t.
In injured at 7 d.a.t.
In injured at 14 d.a.t.
Cell diameter (μm)
n.s.
j
Cells with process overlap (%)

Figure 2.

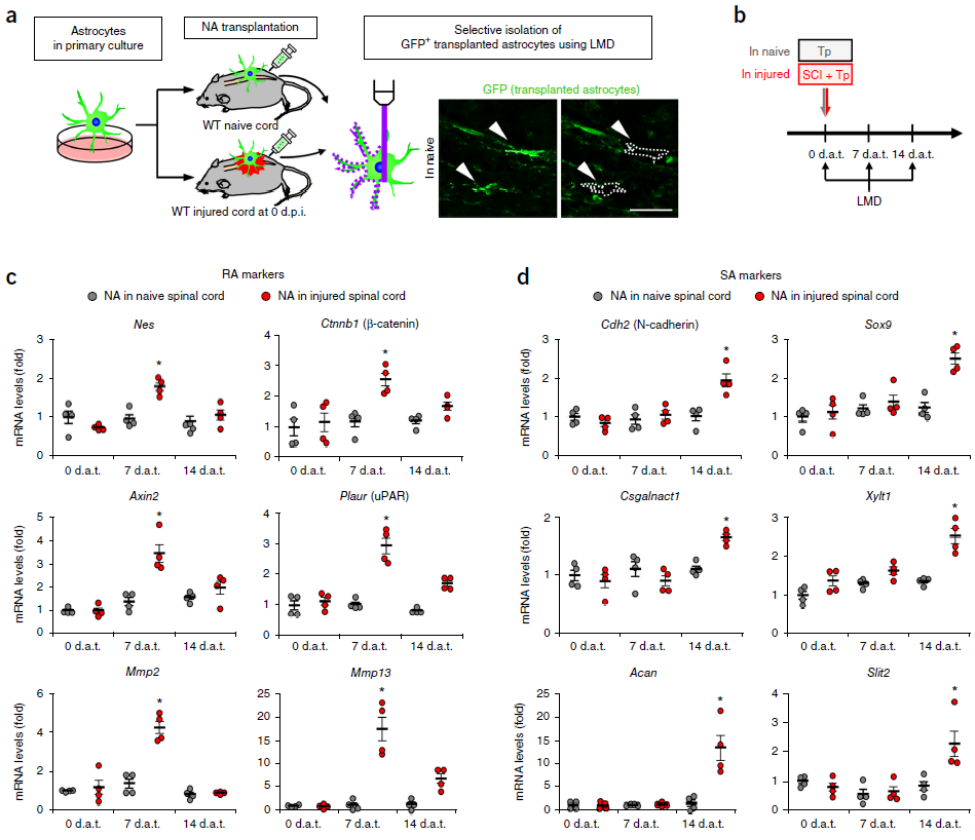
a
Astrocytes in primary culture
NA transplantation
WT naive cord
WT injured cord at 0 d.p.i.
Selective isolation of GFP+ transplanted astrocytes using LMD
GFP (transplanted astrocytes)
In naive
b
In naive
Tp
In injured
SCI + Tp
0 d.a.t. 7 d.a.t. 14 d.a.t.
LMD
c
RA markers
NA in naive spinal cord
NA in injured spinal cord
Nes
Ctnnb1 (β-catenin)
Axin2
Plaur (uPAR)
Mmp2
Mmp13
mRNA levels (fold)
0 d.a.t.
7 d.a.t.
14 d.a.t.
d
SA markers
Cdh2 (N-cadherin)
Sox9
Csgalnact1
Xylt1
Acan
Slit2

Figure 3.

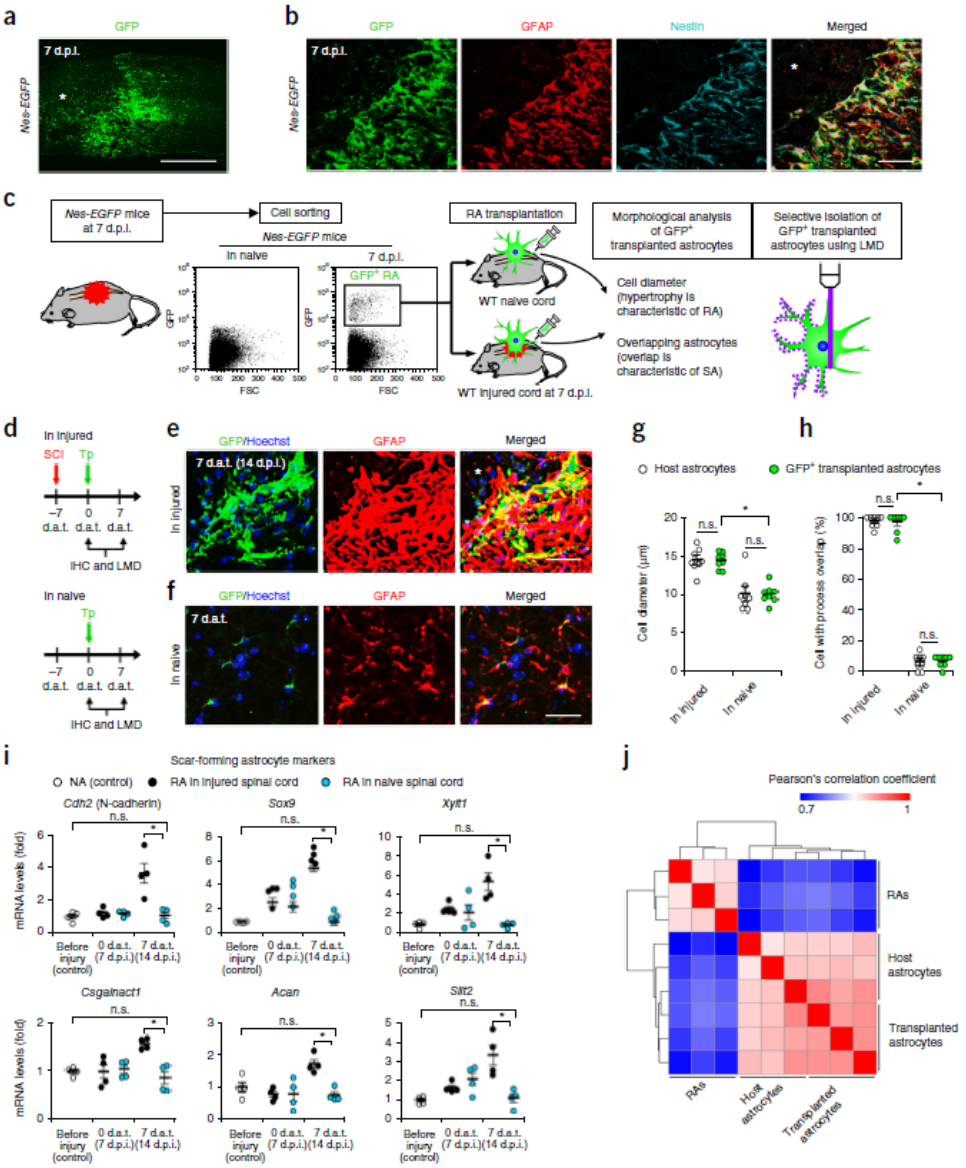
a
GFP
7 d.p.i.
Nes-EGFP
b
GFP
GFAP
Nestin
Merged
7 d.p.i.
Nes-EGFP
c
Nes-EGFP mice at 7 d.p.i.
Cell sorting
Nes-EGFP mice
In naive
7 d.p.i.
GFP+ RA
FSC
RA transplantation
WT naive cord
WT injured cord at 7 d.p.i.
Morphological analysis of GFP+ transplanted astrocytes
Selective isolation of GFP+ transplanted astrocytes using LMD
Cell diameter (hypertrophy is characteristic of RA)
Overlapping astrocytes (overlap is characteristic of SA)
d
In injured
SCI
Tp
–7 d.a.t.
0 d.a.t.
7 d.a.t.
IHC and LMD
In naive
Tp
IHC and LMD
e
GFP/Hoechst
GFAP
Merged
7 d.a.t. (14 d.p.i.)
In injured
f
GFP/Hoechst
GFAP
Merged
7 d.a.t.
In naive
g
Host astrocytes
GFP+ transplanted astrocytes
Cell diameter (µm)
n.s.
In injured
In naive
h
Cell with process overlap (%)
n.s.
In injured
In naive
i
Scar-forming astrocyte markers
NA (control)
RA in injured spinal cord
RA in naive spinal cord
Cdh2 (N-cadherin)
Sox9
Xylt1
Csgalnact1
Acan
Slit2
mRNA levels (fold)
n.s.
Before injury (control)
0 d.a.t. (7 d.p.i.)
7 d.a.t. (14 d.p.i.)
j
Pearson's correlation coefficient
0.7
1
RAs
Host astrocytes
Transplanted astrocytes

Figure 4.

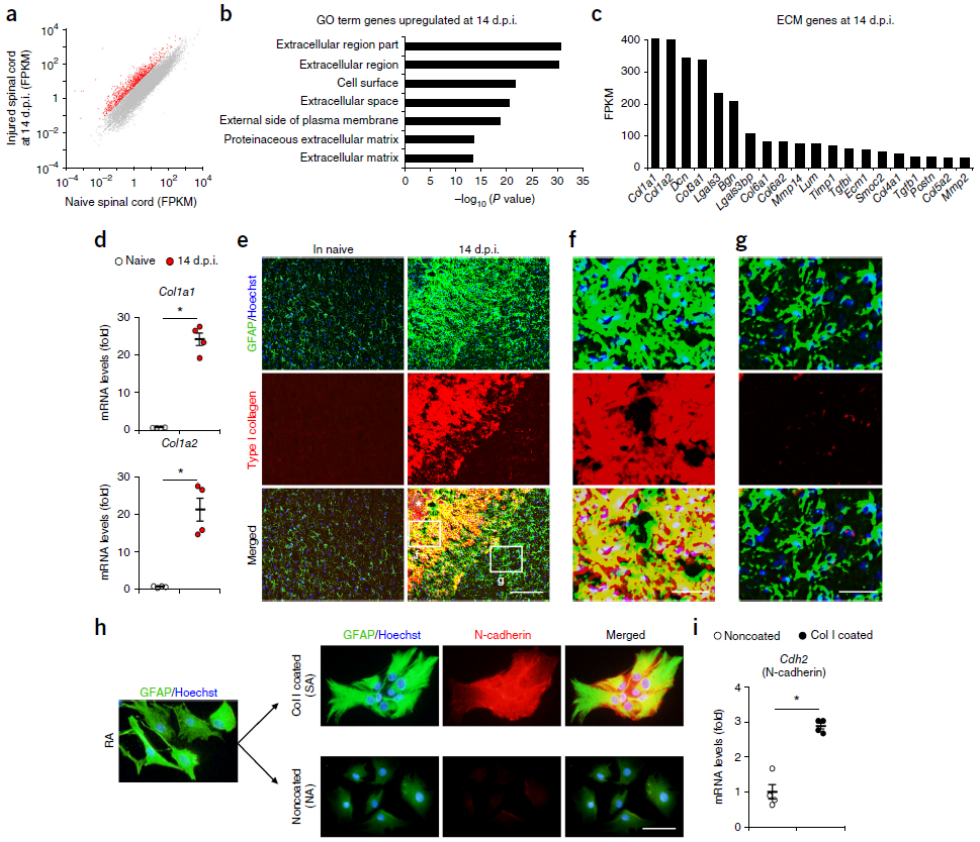
a
Injured spinal cord at 14 d.p.i. (FPKM)
Naive spinal cord (FPKM)
b
GO term genes upregulated at 14 d.p.i.
Extracellular region part
Extracellular region
Cell surface
Extracellular space
External side of plasma membrane
Proteinaceous extracellular matrix
Extracellular matrix
−log10 (P value)
c
ECM genes at 14 d.p.i.
FPKM
Col1a1
Col1a2
Bcn
Col6a1
Lgals3
Bgn
Lgals3bp
Col6a1
Col6a2
Mmp14
Lum
Timp1
Tgfbi
Ecm1
Smoc2
Col4a1
Tgfb1
Postn
Col5a2
Mmp2
d
Naive
14 d.p.i.
Col1a1
mRNA levels (fold)
Col1a2
e
In naive
14 d.p.i.
GFAP/Hoechst
Type I collagen
Merged
f
g
h
GFAP/Hoechst
RA
Col I coated (SA)
Noncoated (NA)
GFAP/Hoechst
N-cadherin
Merged
i
Noncoated
Col I coated
Cdh2 (N-cadherin)
mRNA levels (fold)

Figure 5.

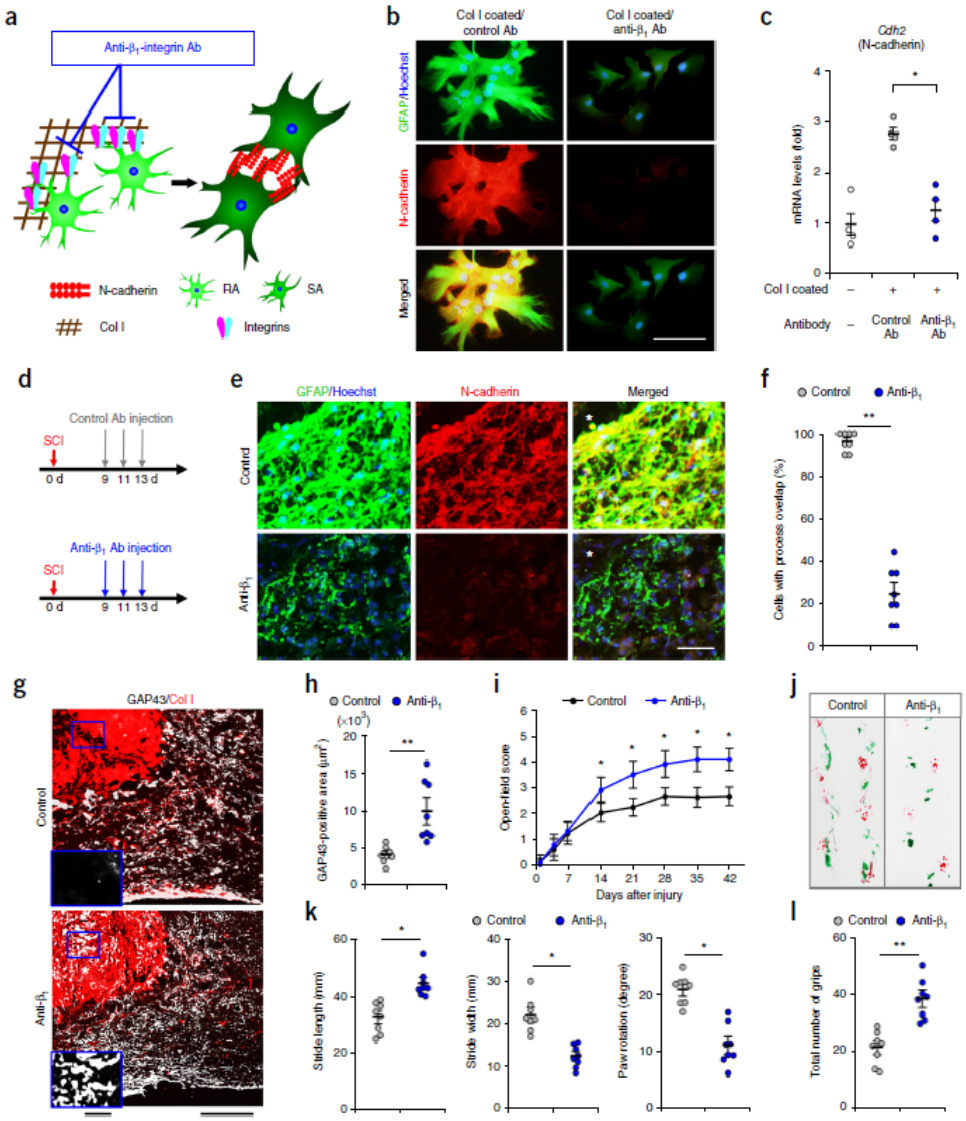
a
Anti-β1-integrin Ab
N-cadherin
RA
SA
Col I
Integrins
b
Col I coated/ control Ab
Col I coated/ anti-β1 Ab
GFAP/Hoechst
N-cadherin
Merged
c
Cdh2 (N-cadherin)
mRNA levels (fold)
Col I coated
Antibody
Control Ab
Anti-β1 Ab
d
Control Ab injection
SCI
0 d
9 11 13 d
Anti-β1 Ab injection
e
GFAP/Hoechst
N-cadherin
Merged
Control
Anti-β1
f
Control
Anti-β1
Cells with process overlap (%)
g
GAP43/Col I
h
GAP43-positive area (μm2)
i
Open-field score
Days after injury
j
k
Stride length (mm)
Stride width (mm)
Paw rotation (degree)
l
Total number of grips

Figure 6.

Supplementary Figure 1

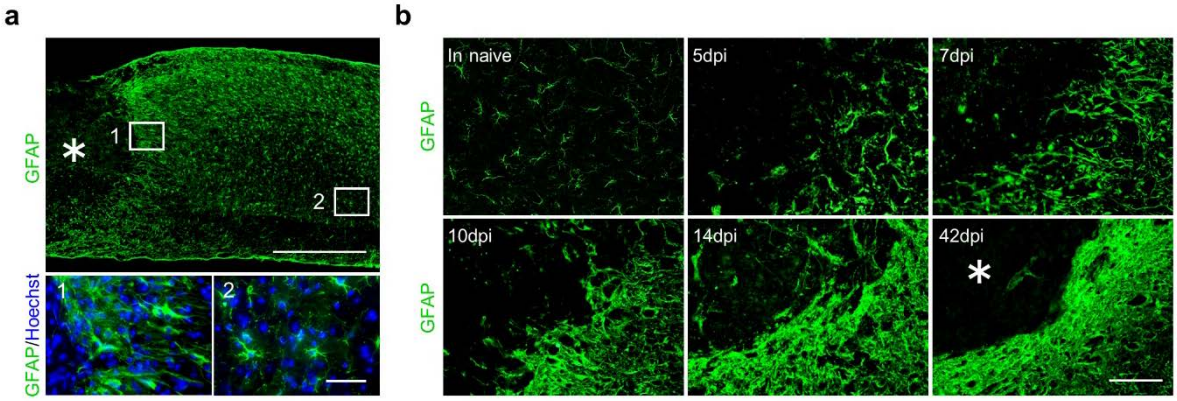

Supplementary Figure 1. Dramatic changes in the astrocytic morphology around the lesion area. (a) Example images depicting GFAP (green) staining of the injured spinal cords at 7 dpi after SCI. The asterisk indicates the lesion epicenter in SCI mice. The inset (1) and (2) are magnifications of the boxed areas in (**a**). Scale bars, 500 μm, insets 50μm. **(b)** Example images depicting time course of GFAP-positive astrocytes (green) before and after SCI. The asterisk indicates the lesion epicenter in SCI mice. Scale bar, 100 μm.

Supplementary Figure 2

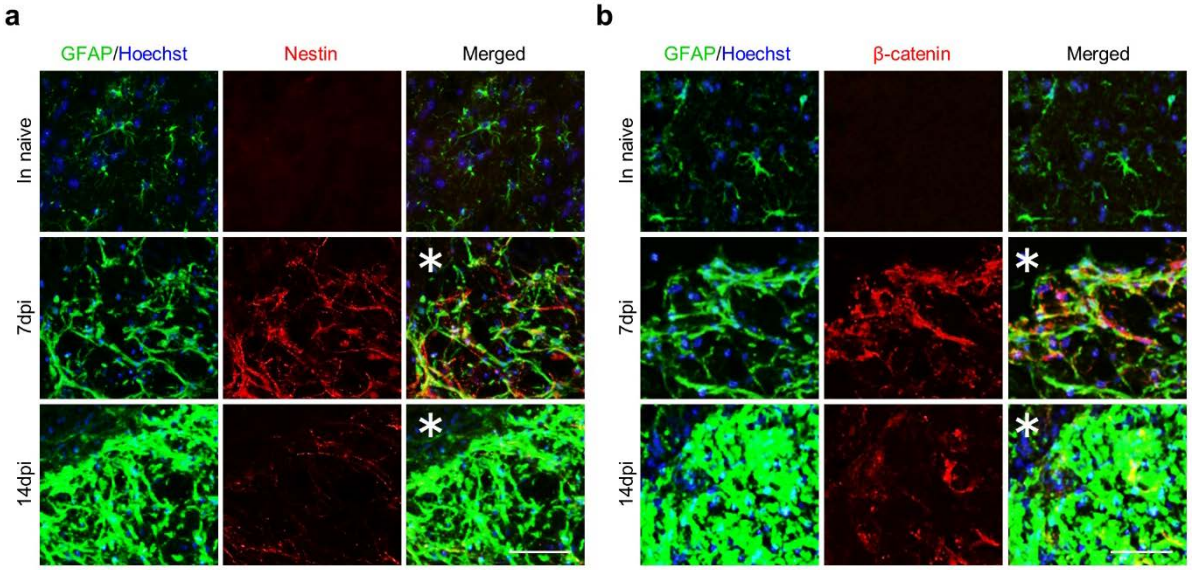

Supplementary Figure 2. RAs expressing their hallmark proteins. (**a** and **b**) Example images depicting immunohistological analysis of the GFAP-positive astrocytes (green) stained with the RA markers Nestin or β-catenin (red) before injury and at 7 and 14 dpi. The nuclei are counterstained with Hoechst (blue). The asterisk indicates the lesion epicenter in SCI mice. Scale bars, 50 μm.

Supplementary Figure 3

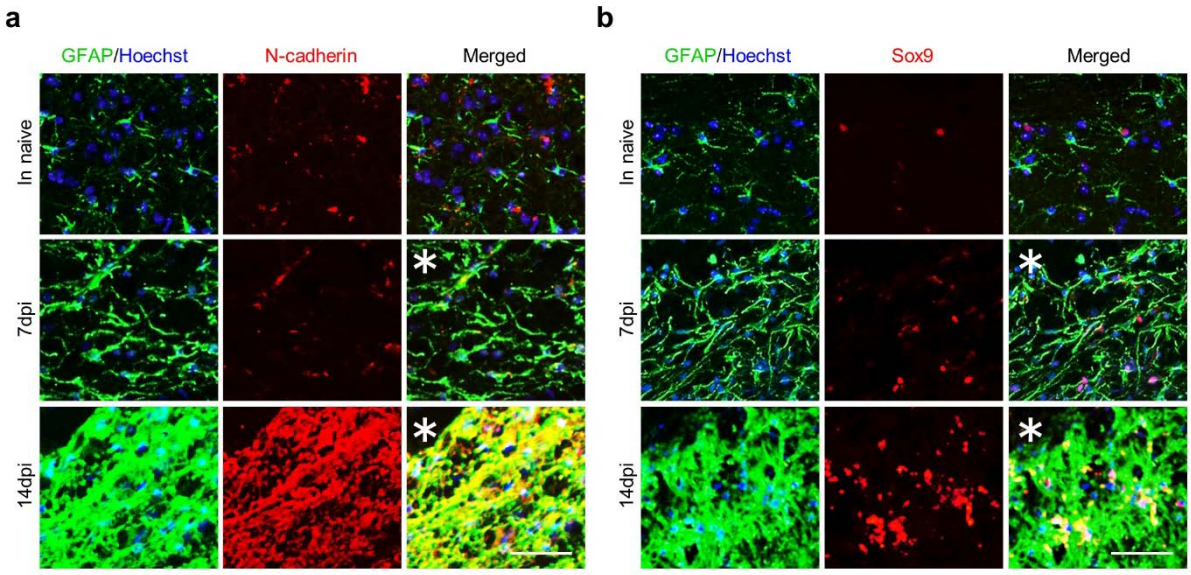

Supplementary Figure 3. SAs expressing their hallmark proteins. (**a** and **b**) Example images depicting immunohistological analysis of the GFAP-positive astrocytes (green) stained with the SA markers N-cadherin or Sox9 (red) before injury and at 7 and 14 dpi. The nuclei are counterstained with Hoechst (blue). The asterisk indicates the lesion epicenter in SCI mice. Scale bars, 50 μm.

Supplementary Figure 4

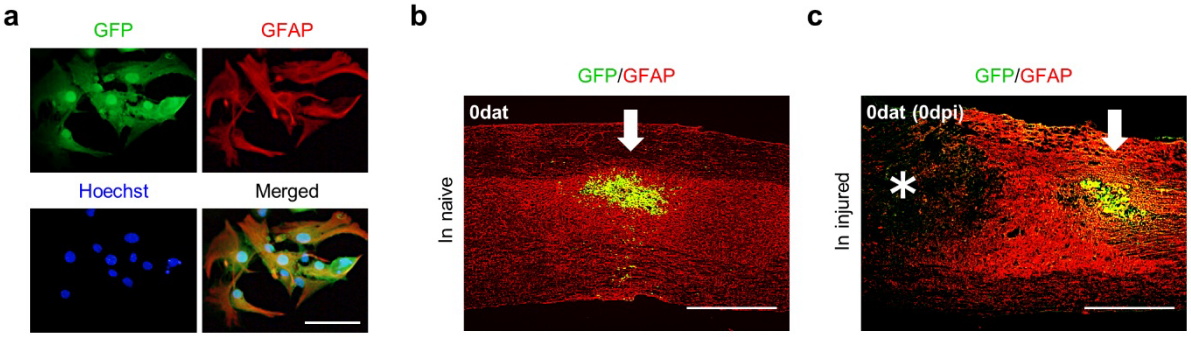

Supplementary Figure 4. Transplantation of NAs into naïve and injured spinal cords. (**a**) Example images depicting immunocytochemical analysis of primary astrocyte cultures prepared from *CAG-EGFP* mice, stained with GFP (green), GFAP (red), and Hoechst (blue). Scale bar, 50 µm. (**b** and **c**) Example images depicting immunostaining of GFP-positive NAs (green) transplanted into the naïve (**b**) and injured spinal cord (**c**) at 0 dat, stained with GFAP (red). The arrows indicate the transplantation points of GFP-positive NAs. The asterisk indicates the lesion epicenter in SCI mice (**c**). Scale bars, 500 µm.

Supplementary Figure 5

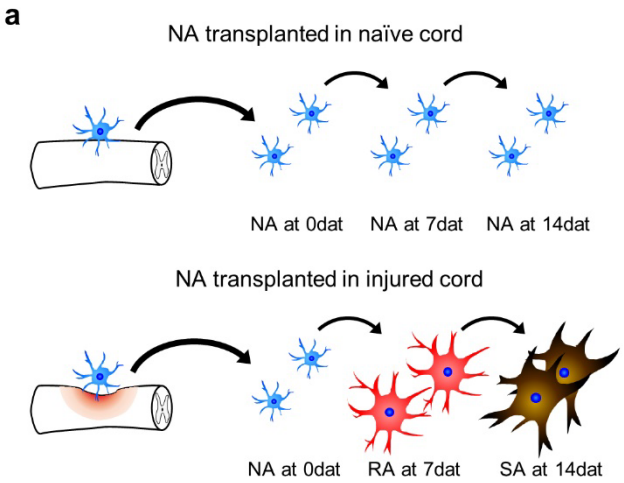

Supplementary Figure 5. Environment-dependent transformation of NAs into naïve and injured spinal cords. (**a**) A schematic representation of the environment-dependent transformation of the grafted NAs.

Supplementary Figure 6

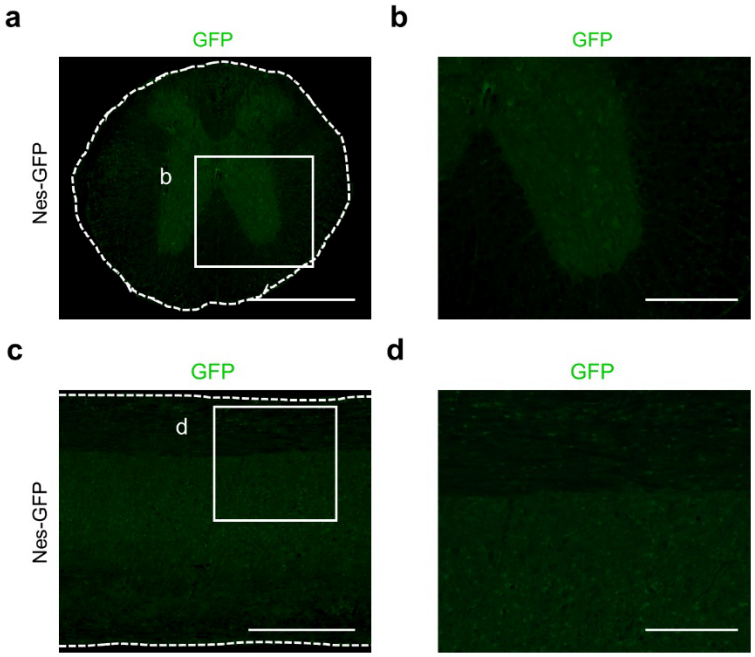

Supplementary Figure 6. No GFP-positive cells in the naïve spinal cord of *Nes-EGFP* mice. (**a-d**) Example images depicting GFP (green) staining of the sagittal (**a** and **b**) and axial (**c** and **d**) sections of the naïve spinal cord of *Nes-EGFP* mice. No GFP-positive cells are present. The images (**b**) and (**d**) are magnifications of the boxed areas in (**a**) and (**c**), respectively. Scale bars, 500 µm (**a** and **c**), 200 µm (**b** and **d**).

Supplementary Figure 7

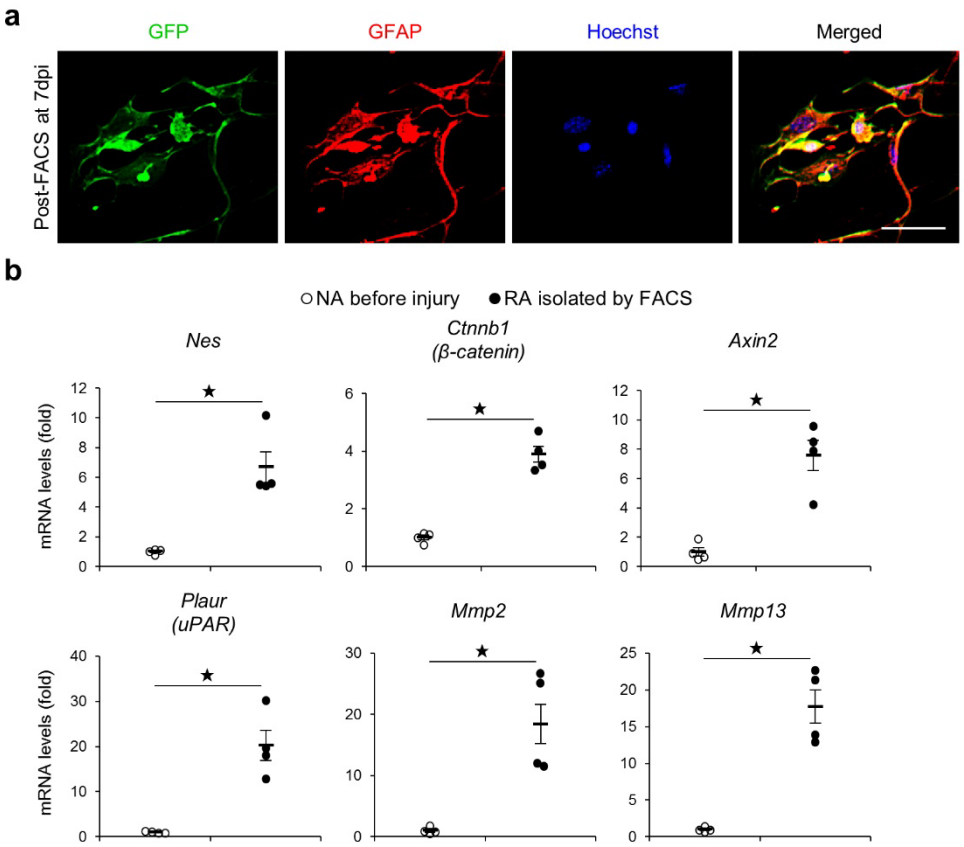

Supplementary Figure 7. The direct isolation and gene expression analysis of GFP-positive RA from *Nes-EGFP* mice. (**a**) Example images depicting immunocytochemical analysis of GFP-positive RAs (green) isolated from the injured spinal cord of *Nes-EGFP* mice at 7 dpi using FACS, stained with GFAP (red) and Hoechst (blue). Scale bar, 50 μm. (**b**) Quantification of mRNA expression levels of RA marker genes in NAs before injury and RAs isolated by FACS (n = 4 mice per group). ★$P < 0.05$, Wilcoxon's rank sum test. Data represent mean ± SEM.

Supplementary Figure 8

a

	# of DEGs
Host astrocytes versus Transplanted astrocytes	0
RAs versus Host astrocytes	2386
RAs versus Transplanted astrocytes	2670

2060 (# of common DEGs)

Supplementary Figure 8. The whole transcriptome analysis of RAs, transplanted astrocytes and host astrocytes. (**a**) The number of significant differentially expressed genes (DEGs) between RAs, transplanted astrocytes and host astrocytes. There were no significant DEGs between transplanted and host astrocytes (with adjusted p-values of < 0.1).

Supplementary Figure 9

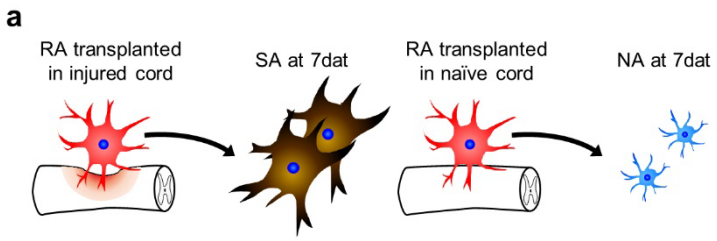

Supplementary Figure 9. Environment-dependent reversibility of reactive astrogliosis. (**a**) A schematic representation of the environment-dependent reversibility of reactive astrogliosis.

Supplementary Figure 10

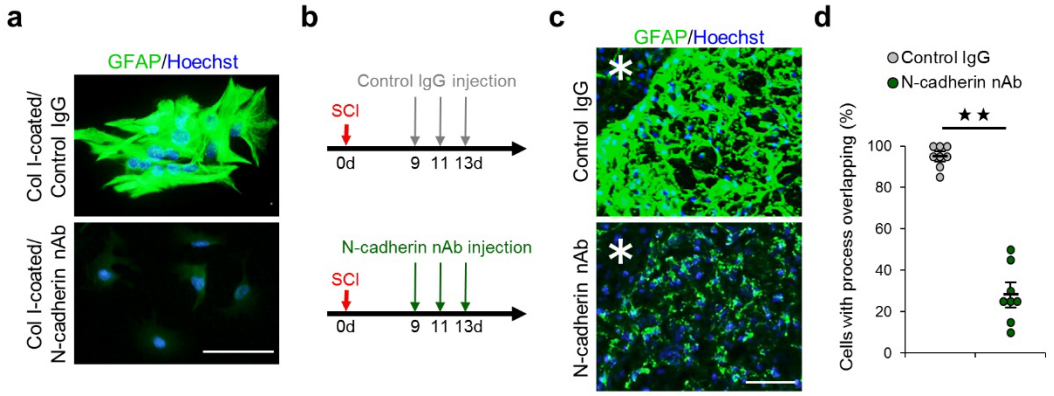

Supplementary Figure 10. The functional blockade of N-cadherin inhibited the transformation of RAs into SAs and attenuated astrocytic scar formation after SCI. (**a**) Example images depicting immunocytochemical analysis of RAs on Col I-coated dishes after the administration of N-cadherin nAb or control IgG, stained with GFAP (green) and Hoechst (blue). Scale bar, 50 μm. (**b**) The schedule of the injections of N-cadherin nAb or control IgG into WT mice after SCI in the *in vivo* experiments. (**c**) Example images depicting immunostaining of the lesion area of the injured spinal cord receiving N-cadherin nAb or control IgG injection at 14 dpi, stained with GFAP (green) and Hoechst (blue). The asterisk indicates the lesion epicenter in SCI mice. Scale bar, 50 μm. (**d**) The ratio of GFAP-positive astrocytes with overlapping of neighboring astrocytic processes (n = 8 mice per group). ★★$P < 0.005$, Wilcoxon's rank sum test. Data represent mean ± SEM.

Supplementary Figure 11

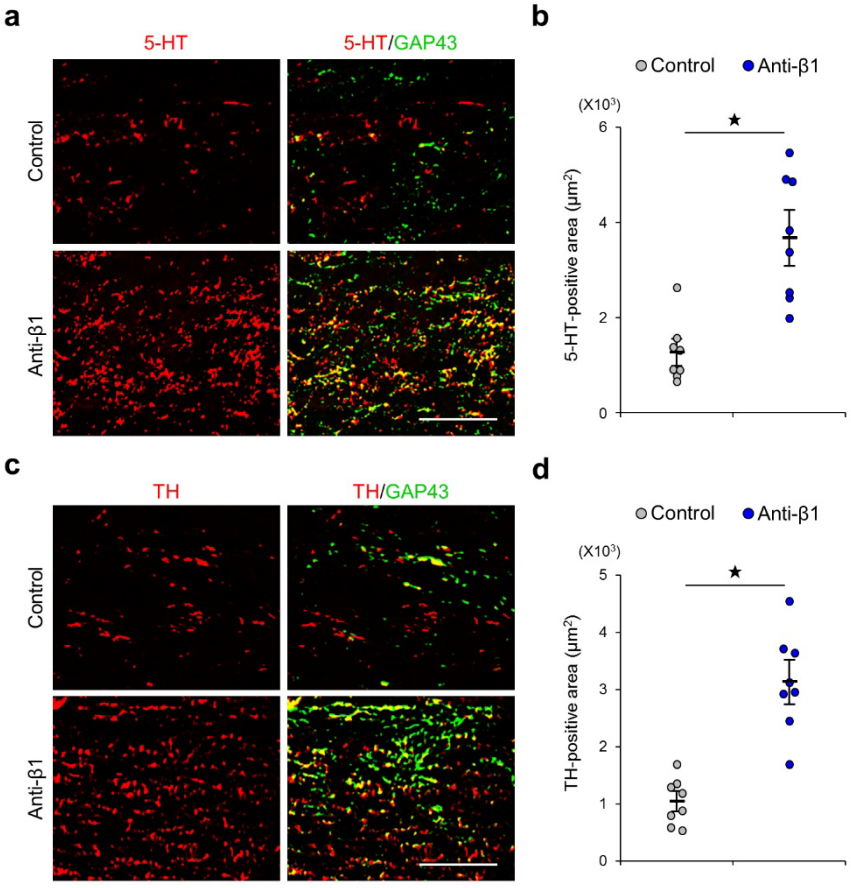

Supplementary Figure 11. Increased numbers of 5-HT-positive and TH-positive axons were observed in the area caudal to the lesion epicenter. (**a** and **c**) Example images depicting immunostaining of the area caudal to the lesion epicenter of the injured spinal cord receiving anti-β1 Ab or control Ab injection at 42 dpi, stained with GAP43 (green) and 5-HT or TH (red). Scale bars, 100 μm. (**b** and **d**) Quantification of the 5-HT-positive or TH-positive area per 4.0 × 10^5 μm^2 (n = 8 mice per group). ★P < 0.05, Wilcoxon's rank sum test. Data represent mean ± SEM.

Supplementary Figure 12

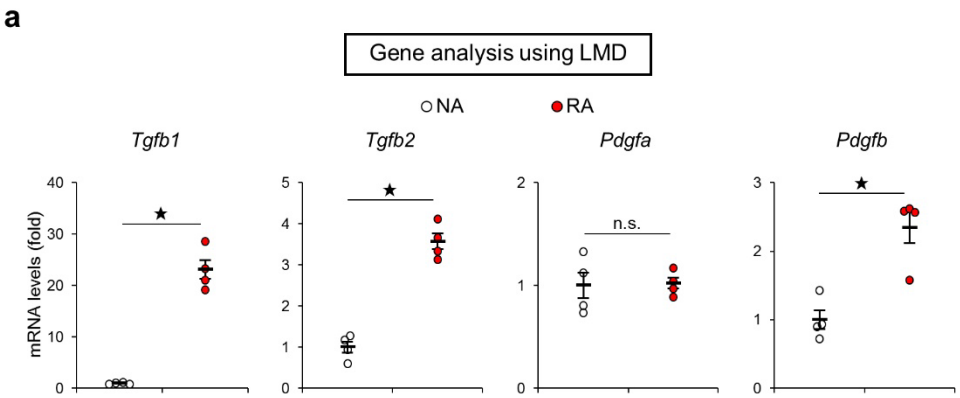

Supplementary Figure 12. Upregulation of neuroprotective factors in RAs. (**a**) Quantification of mRNA expression levels of *Tgfb1, Tgfb2, Pdgfa*, and *Pdgfb* in NAs and RAs (n = 4 mice per group). ★$P < 0.05$, Wilcoxon's rank sum test. Data represent mean ± SEM.

Supplementary Figure 13

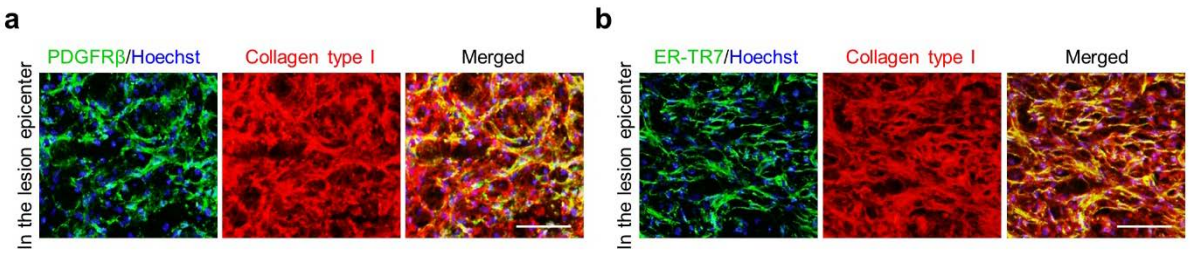

Supplementary Figure 13. Pericytes and fibroblasts produced Col I in the lesion epicenter after SCI. (**a** and **b**) Example images depicting immunohistochemical analysis of the injured spinal cord of WT mice at 14 dpi, stained with collagen type I (red), Hoechst (blue), and PDGFRβ or ER-TR7 (green). Scale bars, 50 μm.

Supplementary Table 1

Primers used for qPCR

Gene symbol	Accession number	5'- Forward primer -3'	5'- Reverse primer -3'
Acan	NM_007424.2	tttgatttcccaccgtgcctttcc	ttcctggtcctgtcttctttcagc
Axin2	NM_015732.4	gagaagtttggattgctgtccacg	acccatttctgcatgtgtcgatgg
Bcan	NM_001109758.1	aattctgctgaaggctcaatgccc	cggaagtgacagaatggaagatcc
Cdh2	NM_007664.4	tacgcagctggttgcagataaagg	tctgcactcctccatagtctatgc
Chst11	NM_021439.2	gttctggtgaagtccacaaactgc	tgtcaccatgggattctacacacg
Cnpase	NM_001146318.1	aaatggcagaccagtatcagtacc	gtctcagaactctttttggtcagg
Col1a1	NM_007742.3	catggagacaggtcagacctgtgt	ggacattaggcgcaggaaggtcag
Col1a2	NM_007743.2	atccaac taagtctcct cccttgg	ggcttctgacta tcttccacag ag
Csgalnact1	NM_001252623.1	cttgagacagtcttgtcacagagc	cagtccttagatcagatctccagg
Ctnnb1	NM_001165902.1	gggtgaatactttactctgcctgc	gtataacgctgcaaaagctgtggc
Gapdh	NM_008084.3	gacttcaacagcaactcccactct	ggtttcttactccttggaggccat
Gfap	NM_001131020.1	tgtactaacagagcgagcctatgc	gggacttgctgcctttaacattgg
Iba1	NM_019467.2	caaagaacacaagaggccaactgg	ttccatgctgctgtcatcagaagc
Mmp13	NM_008607.2	gagagcttagttctgtgaacgagc	aaagcagatggaccccatgtttgc
Mmp2	NM_008610.2	ctatcatcttcatcgctgcacacc	gtacagtcagcacctttctttggg
Mmp9	NM_013599.3	aaggtattcagttgcccctactgg	acacggagaatctctgagcaatcc
Nefh	NM_010904.3	tagcaagagaagataaccctgagc	tcatctgtcagttggacatacagg
Nes	NM_016701.3	gtcagctgagcctatagttcaacg	agagtcactcatcattgctgctcc
Pcan	NM_001081306.1	taatggtgcagctttgcctgatgg	cctgacagtaactcattctgctgc
Pdgfa	NM_008808.3	agacagatgtgaggtgagatgagc	acggaggagaacaaagaccgcacg
Pdgfb	NM_011057.3	tacctccactctgtgtcttcttcc	catcccattacaaccttgctcacc
Plaur	NM_011113.3	tctggatcttcagagctttccacc	cttacggtataactccggtttccc
Slit2	NM_001291227.1	cgtctctagaagcttctagcttcg	tgtaggggagctttagtacaagc
Sox9	NM_011448.4	gaaggtaacgattgctgggattcc	cgtcctccatgttaactctgaagg
Tgfb1	NM_011577.1	gtgacagcaaagataacaaactcc	gagctgaagcaatagttggtatcc
Tgfb2	NM_009367.3	tctgagattacagcaacaacaacc	caatacgtacaactccactgaacg
Vim	NM_011701.4	tgctaactaccaggacactattgg	aggttagtttctctcaggttcagg
Xylt1	NM_175645.3	cagtgaagattctccatcactggg	tctggaaactctgctccatgtagg